SiC-ENABLED MEDIUM VOLTAGE ISOLATED DC-DC CONVERTER BASED

POWER OPTIMIZER FOR LARGE PHOTOVOLTAIC PARKS

by

Sai Kiran Voruganti

APPROVED BY SUPERVISORY COMMITTEE:

_____

Dr. Ghanshyamsinh Gohil, Chair

_____

Dr. Babak Fahimi

_____

Dr. Bilal Akin

To life as I have known it for the past 24 years and to the people in it

SiC-ENABLED MEDIUM VOLTAGE ISOLATED DC-DC CONVERTER BASED

POWER OPTIMIZER FOR LARGE PHOTOVOLTAIC PARKS

by

SAI KIRAN VORUGANTI, B.TECH.

THESIS

Presented to the Faculty of

The University of Texas at Dallas

in Partial Fulfillment

of the Requirements

for the Degree of

MASTER OF SCIENCE IN

ELECTRICAL ENGINEERING

THE UNIVERSITY OF TEXAS AT DALLAS

August 2020

ACKNOWLEDGMENTS

SiC-ENABLED MEDIUM VOLTAGE ISOLATED DC-DC CONVERTER BASED

POWER OPTIMIZER FOR LARGE PHOTOVOLTAIC PARKS

Sai Kiran Voruganti, MS
The University of Texas at Dallas, 2020

Supervising Professor: Dr. Ghanshyamsinh Gohil

DC architecture with an MVDC collection network is advantageous for Photovoltaic (PV) farms in reducing the capital by almost 25% and increase the revenue. Resonant converter is one of the most suitable topologies to realize the low voltage to medium voltage DC-DC conversion. This thesis deals with the design of a Medium voltage isolated LLC resonant converter. The converter is going to be first one of its kind by using medium voltage (10 kV) SiC devices on the medium voltage side of the converter. SiC devices enable very high frequency operation of the converter which leads to reduction in component size thus increasing power density. The design of resonant tank and the transformer is vital in improving the converter efficiency. Existing optimization techniques of resonant converters address either efficiency or power density of the converter as their objectives significantly influenced by intuition and unjustified parametric choices. To optimize the converter design achieving maximum efficiency at a significantly reduced volume, a multi-objective design optimization algorithm is being developed as a part of the thesis. A prototype for 1100V – 7000V, 25kW LLC resonant converter was also built which will be explained in detailed in coming chapters.

TABLE OF CONTENTS

LIST OF FIGURES

LIST OF TABLES

CHAPTER 1

INTRODUCTION

1.1   Renewable energy trends and challenges

Growing interests in Renewable energy because of global climate change and fossil fuel depletion have driven enormous investments in sustainable energy like Solar, Wind, Hydro and Bio energy generation. During the past decade (2010-19), $2.6 trillion was invested in renewable energy globally [1]. The estimate excludes large hydro plants started during the same period. Out of the said total, Solar energy stands first attracting $1.3 trillion followed by Wind energy securing $1 trillion in investments. Country wise investment trends are discussed in [1]. Figure 1 depicts Solar energy investments out of all the investments in renewables during the last decade.

Percentage of total investments

■ Solar   ■ Others
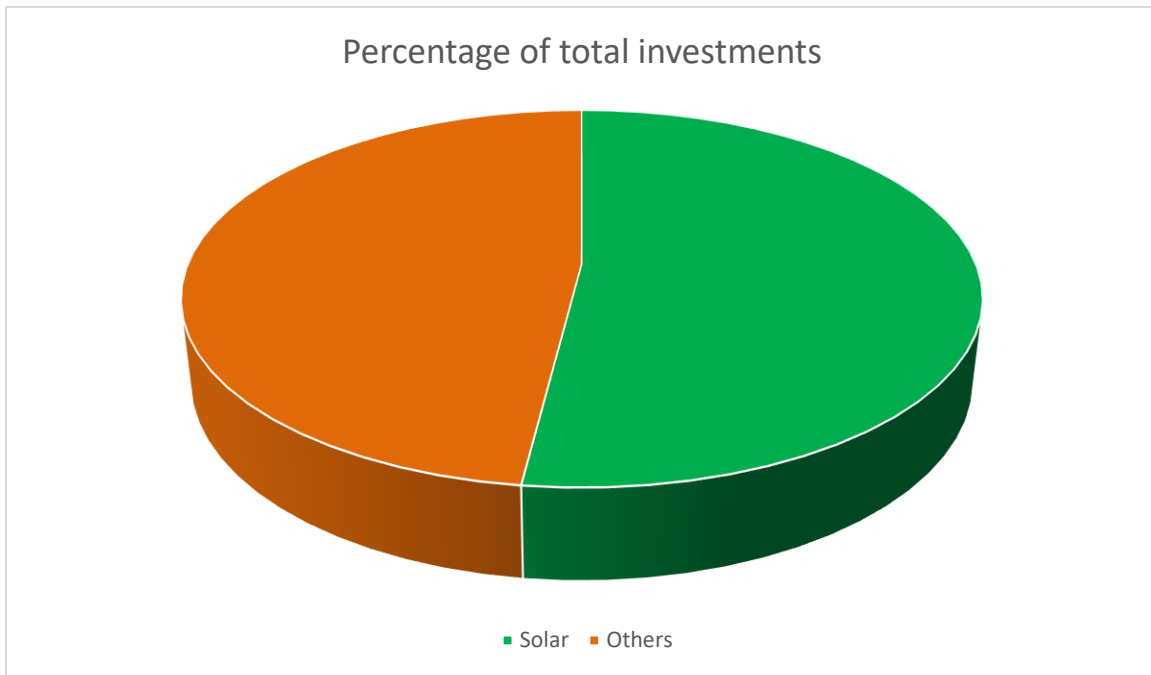
Figure 1: Investments in different renewable energy sectors

There has been 25.52 times rise in installed capacity of Solar energy globally during this period. The levelized cost of electricity for solar energy has come down globally by 81% which excludes the cost of tracking systems [1].
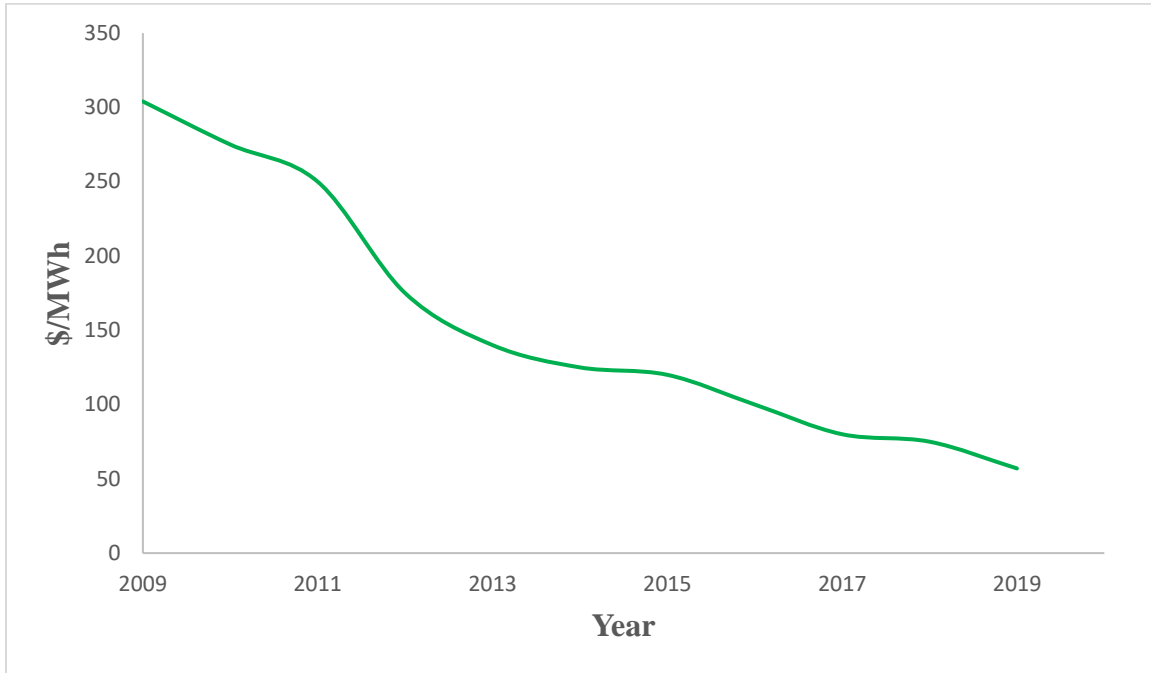
Figure 2: Levelized cost of electricity-Solar energy

Figure 2 represents the change in levelized cost of electricity of Solar energy from 2009 to 2019 in $/MWh. The cost came down from $304 to $57. This reduction is mostly because of financial, operational factors, improved efficiency of the PV panels and some other factors which do not include the tracking or collection and transmission technology advancements. Though both, interests and the investments are increasing, the amount of electricity generated from solar energy is still very small (around 2% of global energy generation) compared to fossil fuel powered generation globally.

[2] gives a good comparison between DC and AC collector grids for wind parks. Increased costs, reliability and protection are few major concerns with DC collection when compared to AC

collection [3]. Faults including critical SC faults and cable-ground faults in DC collection for wind farms were discussed and methods were proposed to mitigate them in [4]. Application of DC collection to PV parks has not been equivocally discussed in the available literature compared to AC collection. A configuration which is proposed in [5] has module-level Maximum Power Point Tracking (MPPT) converters connected to a common low voltage DC bus which feeds inverters that are connected to the grid. Though this approach has its own advantages of DC collection, the cost aspect and reliability can still be significantly improved. Two medium voltage level DC (MVDC) collector configurations for PV were proposed and compared with existing medium voltage AC (MVAC) collector configuration in [6]. The DC configuration 2 proposed in [6] outperformed both the DC configuration 1 and the AC configuration. Detailed economic viability comparison of all those three configurations is discussed in [7] with cost modeling, analysis for a year of measured weather data of two different locations using Monte Carlo method.

The configuration proposed in this work is very similar to the DC2 configuration discussed in [7]. The primary objective of this thesis is to bring down the Levelized Cost of Electricity (LCOE) significantly using the proposed MVDC collection method for large PV parks. To achieve significant reduction in LCOE, existing power grid architecture needs some radical changes. Existing AC collection network which typically consists of a low voltage subfield inverter followed by a line frequency transformer and a robust fault protection system is an outcome of years of research efforts. DC collection for multi-MW to GW PV parks also requires enormous efforts and innovations to arrive at a competitive LCOE. At the same time, it is not valid to state that this evolution requires similar timeline as that of AC collection. MVDC collection using

3

isolated DC-DC converters is promising when it comes to the LCOE reduction due to improved

plant efficiency and reduction in the COM (Capital, Operation & Maintenance) costs.

The EPC (Engineering, Procurement & Construction) cost breakdown for large PV parks

reveals that the expenditure on cables, transformers, combiner boxes, labor etc., add up to a total

of 24% of the capital whereas the inverters contribute to 7.5% [8]. This gives an opportunity to

reduce the LCOE using an isolated MV DC-DC converter which can also perform MPPT. The

components of LCOE that can be reduced using the proposed configuration are as follows
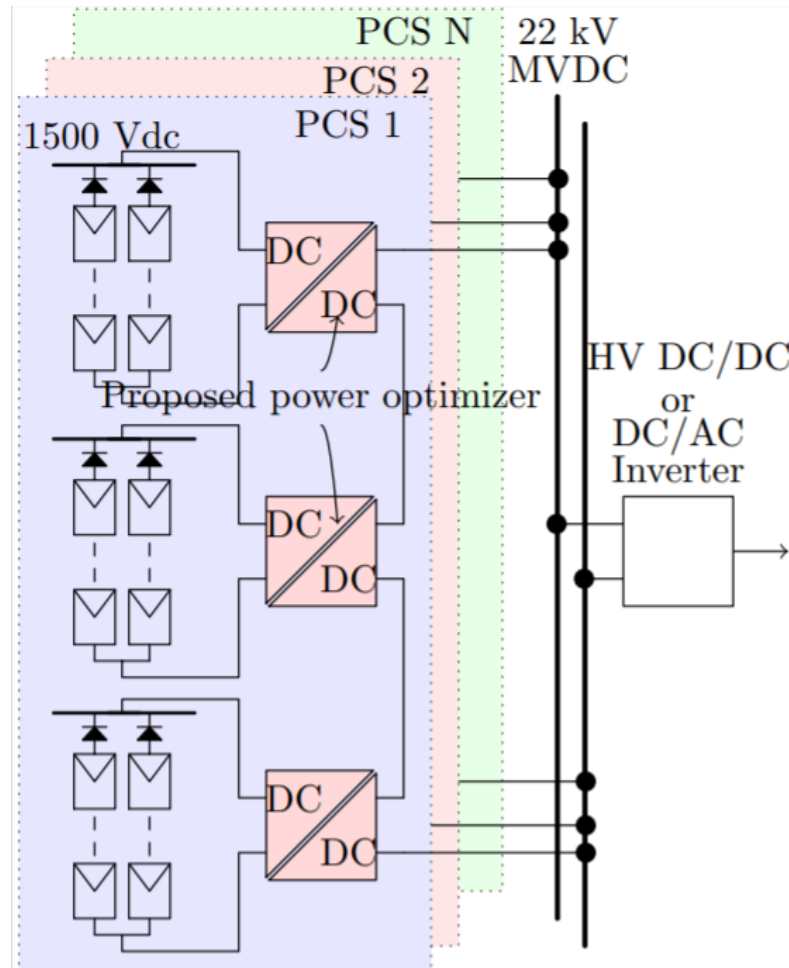
Figure 3: Proposed MVDC Collection for large PV parks

- **Capital & installation:** Cost of capital and installation can be reduced due to elimination of line frequency transformers and labor costs associated, reduction in cable costs, cable conduits and combiners.

- **Improving the revenue generation:** One of the advantages of the proposed configuration is having active semi-conductor devices that can be soft switched resulting in nearly negligible switching losses compared to the installed power capacity. The elimination of line frequency transformers in the LV power stages leads to increased overall efficiency of the system which in turn increases the generated revenue.

Figure 3 represents the proposed configuration with LLC resonant based isolated DC-DC converter for the MVDC collection. Using the LLC resonant converter provides an ability for both the low and medium voltage semi-conductor devices to be soft switched and this configuration also enables EMI reduction [9]. This gives an advantage of improved efficiency and higher operating frequencies. The MPPT voltage variation of the PV strings is significant, subject to different parameters like temperature, partial shading etc. This variation in the MPPT voltage can be handled by control by varying the frequency which in turn changes the gain of the resonant tank. Thus, the resonant converter will be operating with a wide variation of the input voltage. Few challenges involved in designing resonant converters for such applications with wide input voltage variation are choice of resonant tank parameters, optimal design of the high frequency transformer for a wide range of frequency variation etc. Multi-objective optimization is chosen to obtain the optimal converter design for this application whose objectives and other functions will be discussed in the coming sections of this thesis. One of the optimal designs is also chosen to validate the approach and analysis.

1.2   Outline of the thesis

Chapter 2: Types of resonant converters, advantages & disadvantages of LLC resonant converter, analysis methods and design procedure using the analysis.

Chapter 3: This chapter includes the discussion about Multi-objective optimization using a simulation-based approach, a genetic algorithm-based approach, and its structure. Mathematical modeling of different converter parameters required for the optimization, results from the optimization, and the analysis of a selected design.

Chapter 4: Steps involved in the development and fabrication of different converter stages, considerations for different component selection, assembly process, test conditions and results are discussed in this chapter.

Chapter 5: This includes the summary of the objective, approach results and highlights of this work. Improvements that can be made and future scope of this work are also discussed in this section.

CHAPTER 2

LLC RESONANT CONVERTER

2.1 Resonant Converters

Resonant converters have existed for many years now but recent attention towards them is because many applications like consumer electronics, battery charging etc., now require increased efficiencies and power densities due to continually changing regulations and standards. In applications that require wide range of load and voltage regulation, the choice of topology to optimize the efficiency and power density comes with significant challenges.

Series resonant converter (SRC) and Parallel resonant converter (PRC) are two widely used configurations of the two-element based resonant tank combinations. One of the major drawbacks of using an SRC is the maximum gain of its resonant tank which is unity. Based on the operating frequency, a resonant converter can achieve either Zero Voltage Switching (ZVS) or Zero Current Switching (ZCS) of the semi-conductor devices. ZVS is attainable when the impedance of the resonant tank is inductive in nature and ZCS when the impedance is capacitive. It is usually preferable to operate a resonant converter in inductive region. When operating in capacitive region i.e., when the operating frequency is below the resonant frequency, a higher order component of the low frequency input to the resonant tank might match with the tank's resonance. At this point the predictable relationship between the frequency and gain of the resonant tank is no longer valid. So, the capacitive region is generally avoided. Theoretically, the gain curve of an SRC is flat at no load condition and the slope of the gain curve increases with load. This means that, to regulate an input voltage variation, the frequency variation in an SRC decreases with increase in load. On the other hand, the maximum gain offered by the resonant tank in a PRC is load dependent. The

7

maximum frequency and peak gain offered by a PRC decrease with increase in load. The gain characteristics of a PRC are opposite to that of an SRC. The slope of it decreases with increasing load. An LLC resonant converter combines the advantages of both SRC and a PRC. It can be operated in the inductive region to obtain ZVS as in an SRC and it can also offer gains both higher and lower than unity as in PRC.

2.2   LLC Resonant Converter

LLC converter is one of the resonant tank combinations available with three or more L & C elements widely used in numerous applications [10, 11, 12, 13]. Advantages of LLC resonant converter are soft switching over a wide operating range, synchronous rectification of the rectifier stage devices etc., leading to negligible switching losses which enables high switching frequency operation leading to higher power densities. It is difficult to classify all the resonant converters because many combinations are possible based on the type of switching network, number of elements in the resonant tank and their configuration [14]. The configuration under discussion is an isolated LLC based resonant converter which is different from a conventional resonant converter by having an isolation transformer. This transformer not only provides galvanic isolation, but it also steps the voltage level up or down based on the requirement of the application. There are thirty six different resonant tank configurations with three reactive tank elements but of them, only fifteen are practical with a voltage source as an input [15].

The block diagram of resonant converter under discussion can be referred from Figure 4. It consists of a full bridge inverter followed by an LLC resonant tank which feeds the transformer. The output of the transformer is fed to a half-bridge rectifier that transfers the power to the MV grid. Since the MPPT voltage of the PV array is subject to many variables and varies on a wide

8

range, the resonant converter must operate over a wide input variation. One of the main reasons LLC topology is chosen is because of its ability to provide a wide range of gain without compromising on the advantages that a three-element resonant converter can offer. A frequency modulation control is considered in this work, where frequency of the square wave output of the inverter is varied to keep the output voltage constant for any MPPT voltage input. The change in frequency around the resonant tank circuit's resonant frequency ensures the power flow.
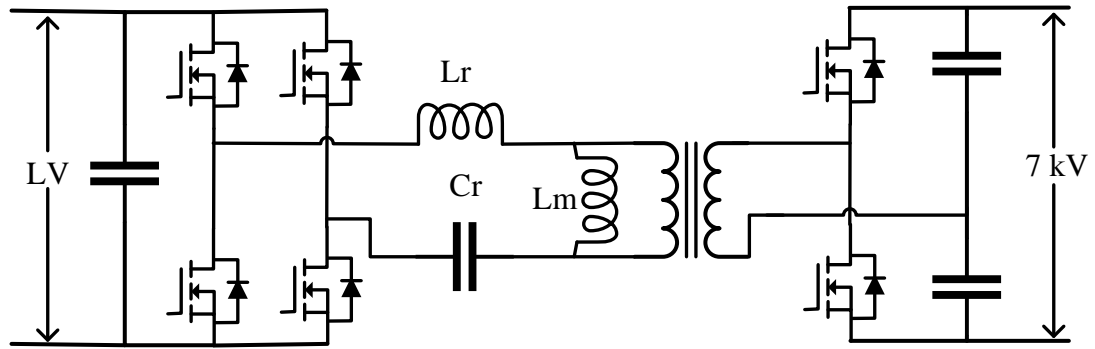
Figure 4: LLC Resonant converter with half-bridge secondary rectifier

There are various approaches to analyze different operating modes and characteristics of the converter at different conditions. One can divide the analysis methods into three types which are time domain, frequency domain and state-plane method. First Harmonic Analysis (FHA), a frequency domain method is considered to analyze the converter dynamics. Though FHA is not very accurate at frequencies away from resonant frequency, it is chosen because it is not computationally complex as other approaches. One of the main reasons the resonant converters are still limited to only a few applications is that limited information is available on how the converter operates under different conditions. The steady-state analysis of the LLC resonant converter is discussed in [16] & [17].

2.3 FHA based steady-state analysis of the LLC resonant converter

Fundamental Harmonic Analysis (FHA) was proposed by R. L. Steigerwald in 1988 [18]. It is a frequency domain analysis method. As shown in Figure 4, the input to the resonant tank is a square-wave voltage generated by the primary full bridge inverter. In FHA, the fundamental sinusoidal component of this square-wave is considered for the converter analysis and its higher order harmonics are neglected. With three reactive elements in the tank circuit, there are two different resonant frequencies, one when the series inductor (L_r) and capacitor (C_r) resonate at f_o and the second when L_r, C_r and the parallel inductor (L_m) participate in resonance at f_1.

$$f_o = \frac{1}{2\pi\sqrt{L_r C_r}}$$
$$\text{2.1}$$

$$f_1 = \frac{1}{2\pi\sqrt{(L_m + L_r)C_r}}$$
$$\text{2.2}$$

The ratio of L_m to L_r can be defined as L_n is an important design parameter and a part of the resonant tank's gain function which will be discussed further in this section. It is obvious that $f_o > f_1$.

The impedance offered by the resonant tank is inductive for frequencies above f_o and it is capacitive for frequencies below f_1. But for frequency range between f_o and f_1, the impedance can be either inductive or capacitive based on the equivalent load resistance. Since the input to the resonant tank is a square wave AC, an AC equivalent circuit which can be referred from Figure 5 makes the analysis simple. The resistance R_{ac} in the equivalent circuit is not the same as the load resistance and includes the effect of transformer and the rectifier referred to the primary. The value of this AC load resistance can be derived from equation 2.3.

$$R_{ac} = \frac{8n^2 R_o}{\pi^2}$$
$$\text{2.3}$$

10
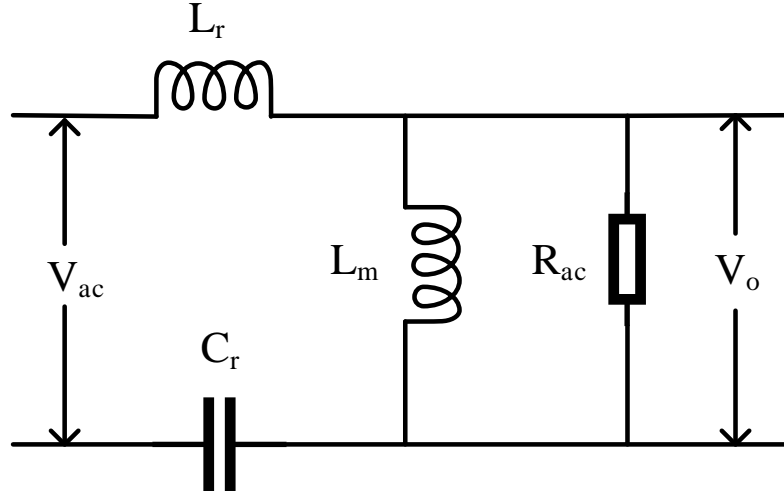
Figure 5: Equivalent AC circuit of the LLC resonant converter

The gain offered by the resonant tank (M) is a function of the switching frequency f_s, the inductors ratio L_n which was discussed earlier and the Quality factor Q_e. Magnitude of M can be found by using the equation 2.4.

$$M = \frac{L_n F_n^2}{\sqrt{\left((L_n + 1)F_n^2 - 1\right)^2 + \left((F_n^2 - 1)F_n Q_e L_n\right)^2}}$$

2.4

Where

$$Q_e = \frac{\sqrt{\frac{L_r}{C_r}}}{R_{ac}}$$

2.5

and

$$F_n = \frac{f_s}{f_o}$$

2.6

F_n is called normalized switching frequency and L_n is called normalized inductance. L_n is a fixed parameter once a design is chosen and F_n and Q_e are two dynamic variables required to

calculate the required gain for a specific operating condition. But during the design stage, all three of them are design variables that can yield millions of resonant tank designs for the same application and are to be chosen carefully. For many applications, boundaries of design space are defined based on intuition and experience which yield good results most of the time. But for the MVDC collection of PV parks, things are not as straightforward as a simple power supply application. Both the MPPT voltage of the PV subfields and the load or power supplied to the grid from a PV park vary over a wide range. The gain characteristics with respect to the switching frequency vary based on the loading condition, as mentioned earlier. For the configuration under discussion, the resonant inductances L_r and L_m are considered to be integrated in the Medium Frequency Transformer (MFT) as its leakage and magnetizing inductances. In such cases, the inductance ratio L_n is also going to have a significant influence in the MFT's size and the overall converter efficiency. The frequency dependent gain characteristics of the resonant tank also vary when L_n is varied but this is during the design stage. The resonant tank gain (M) vs normalized switching frequency (F_n) for different loading conditions (Q_e) at a fixed value of inductance ratio (L_n) can be referred from Figure 6 and the same plot at different values of inductance ratio (L_n) helps us to understand the effect of variation of L_n. Decrease in L_n for a fixed Q_e or decrease in Q_e for a fixed L_n would give higher peak gains and steeper gain curves which means the frequency variation to achieve the same load regulation or voltage regulation would also decrease.
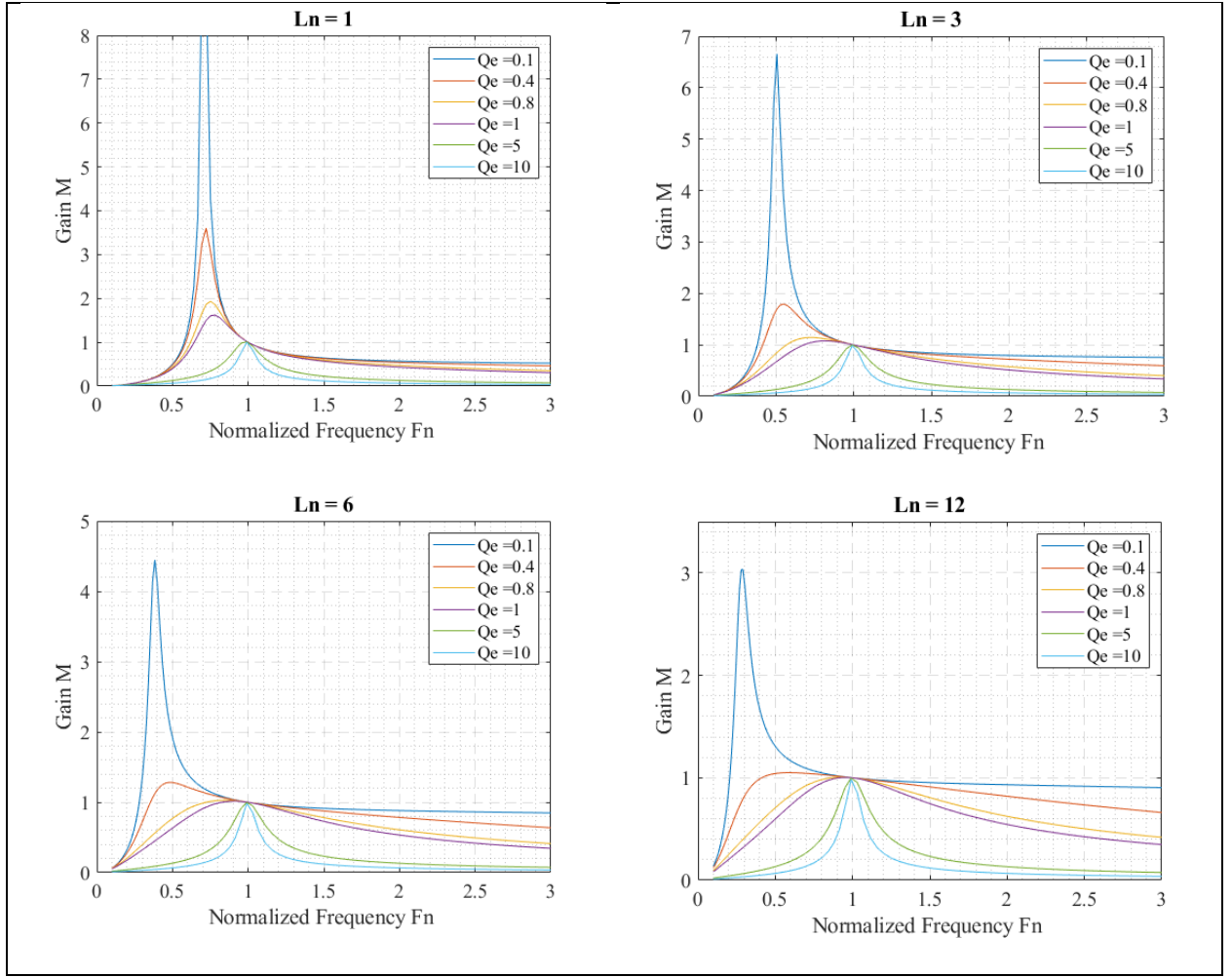
Figure 6: Gain curves for different L_n and Q_e values

Of all the possible combinations, there is one similarity which is the Unity gain point. For any resonant tank configuration and at any loading conditions, ideally, the gain offered by the resonant tank is 1 at resonant frequency f_o. From Figure 6, it can also be inferred that the gain of the resonant tank varies such that the frequency at which the peak gain occurs moves towards the resonant frequency f_o with increase in load or Q_e. Using FHA, when the parasitic components like leakage of secondary winding (L_{lks}), junction capacitance of the secondary-side devices (C_j) and inter-winding capacitance of the transformer are considered, the resonant frequency f_o was observed to be lower than the desired value where the gain is higher than 1 and also rise in gain at

higher switching frequencies [19]. Since FHA considers only the fundamental of the applied square wave voltage and considers the current to be sinusoidal, it's not very accurate in modes when the current is discontinuous or when the input voltage is significantly lower or higher than the nominal voltage. Simulations were performed to observe the change in accuracy of FHA over different operating modes and based on the results, it was decided to add the third harmonic component to the analysis which will be discussed in the next section of this document. Adding the third harmonic component slightly improves the accuracy of the analysis and computationally a good trade-off.

2.4   Design steps of an LLC resonant converter

A general step by step design procedure of an LLC resonant converter is discussed in this section which uses some of the functions and concepts that were already discussed. To design a resonant tank, one must come up with the required converter specifications like input & output voltages, rated output power, switching frequency etc. This design procedure is a generalized approach followed to design power supplies and the changes required in this procedure will be discussed after all the design steps.

The first step is to define the transformer turns ratio (n). This should be done using the nominal input and output voltages $V_{in_{nom}}$ and $V_{o_{nom}}$ of the converter.

$$n = \frac{V_{in_{nom}}}{V_{o_{nom}}/2}$$ 2.7

Since the considered configuration has a half-bridge on the secondary side, the transformer's secondary voltage would be half the output voltage. The next step is to calculate the min. and max. gains that are required from the resonant tank (M_{min} & M_{max}).

14

$$M_{min} = \frac{n\,V_{o\,\min}}{V_{in\,\max}} \quad \& \quad M_{\max} = \frac{nV_{o\,max}}{V_{in\,min}} \tag{2.8}$$

Upon the device selection, the forward voltage drop of the secondary device can also be added to the min. and max. output voltages to calculate the respective gains. After calculating the required gains, the values of L_n and Q_e are to be chosen to obtain the resonant tank parameters. Generally, the choice of these values for a power supply application can be based on existing design references, intuition, or experience. But for applications like MVDC collection where the input voltage and load vary over a wide range, the same approach may not provide optimal values of L_n and Q_e.

For example, a small value of L_n can bring advantages like higher peak gain, steeper gain curves which means the range of operating frequency would be very narrow. But lower L_n leads to higher magnetizing currents which lead to increased losses and reduced efficiencies. On the other hand higher values of L_n can help reduce the magnetizing currents increasing the efficiencies but the range to obtain ZVS can become very narrow and because of increased operating frequency range, the size of the transformer could be higher in such cases. The advantages of having small Q_e can be higher peak gains but the associated frequency range would be larger. Increasing the Q_e can overcome these disadvantages but due to lower peak gains, the design might not be able to provide the required gain in few operating points. The choice of resonant frequency f_o is another design is another variable which is going to directly affect the size of the converter and power density. There are no proper instructions on the choice of these design variables in the existing literature. Thus, Multi-Objective design optimization is chosen to optimally choose the values of L_n, Q_e and f_o.

More details about the optimization algorithm are discussed in the next chapter. Once the optimal values of L_n, Q_e and f_o are obtained, C_r can be calculated by using equations 2.1 and 2.5.

$$C_r = \frac{1}{2\pi f_o Q_e R_{ac}}$$
<div align="right">2.9</div>

Where R_{ac} should be considered for max. loading (for ex. 110 or 120%). L_r and then L_m can be found using C_r. After obtaining the resonant tank parameters, there are more variables in the system like the configuration of primary inverter and secondary rectifier (half-bridge, full-bridge etc.), number of turns of primary and secondary windings of the transformers, transformer core material, and type of wire for the transformer etc. Since the use of LLC resonant converter for MVDC collection is not reported in literature, the choice of different parameters, materials and combinations in this configuration must be justified. The only way these choices can be justified is if one analyses all possible combinations and choses the best one among them. With prototyping out of the scope to optimize, different combinations can be listed out and simulated to obtain the performance which can be used as a basis for comparison to choose the best configuration. Since there are many variables, millions of designs are possible and simulating most of them would be a very complex problem and it could take from days to months to simulate those designs. Also, there are constraints like temperature rise in semi-conductor devices & transformer, max. flux density in the transformer core etc., which must be verified for every design. So, a Mission profile based Multi-objective Optimization is chosen to help reduce the complications in obtaining an optimized design. An algorithm is designed to explore the design space and provide the optimal converter designs as an output. More about the optimization and the algorithm associated will be discussed in the next chapter.

CHAPTER 3

MULTI-OBJECTIVE OPTIMIZATION

3.1   Simulation based optimization approach

Initial approach of this work was to perform a simulation-based optimization using PLECS to evaluate the performance, compare various configurations and choose the best one out of them. With the limited information available in literature, twenty-five different resonant tank combinations corresponding to different L_n and Q_e combinations were chosen as a starting point of the optimization. The value of L_n is varied from 4 to 6 in steps of 0.5 and for each value of L_n, five values of Q_e are chosen in steps of 0.005. The consideration for the choice of Q_e was to make sure that the resultant resonant tank would be able to provide the required gain for the converter to operate over all the operating points. Rest of the converter parameters were calculated for these twenty-five combinations and thus obtained converters are simulated at five different MPPT voltages and twenty-five different power levels keeping the output voltage constant.

This analysis only considered semi-conductor losses to calculate the converter's efficiency at each operating point. The resultant 3125 simulations produced a lot a data that gave information about the operating frequency, converter's efficiency, and junction temperature of each semi-conductor device for every simulation. All this was only for a one resonant frequency. By varying the resonant frequency from 50 kHz to 200 kHz in steps of 10 kHz, the number of simulations required to perform the optimization was 50000. At this point, analyzing all the data obtained from the simulations became impractical. Adding to this, there were cases where some configurations violated the maximum junction temperature constraint at some operating points, but this was known only after the simulations were performed. Few other disadvantages of this approach were:

the simulations did not include the transformer losses, its impact on the converter's efficiency and its temperature rise, the MFT's volume was not being optimized, different core materials and wire types were not being explored to obtain the best version of the MFT for this application. Also, the design space was not being fully explored to optimize the converter design. To overcome these disadvantages, Multi-objective Optimization is chosen to obtain the optimal converter design.

3.2   Genetic algorithm based Multi-objective Optimization

Using the genetic algorithm in MATLAB, Multi-objective Optimization was performed to obtain a set of feasible converter designs to choose from, for the application under consideration. The algorithm is designed to optimize the objective function, which means the algorithm converges when all the objective variables are minimum and satisfy the constraints defined at the same time. The output of the optimization is a Pareto front with all the feasible designs. In this work, the optimization algorithm is designed to yield designs with min. power losses while having a small volume at the same time. Optimization is not a straight-forward process as every iteration requires the analysis of the system's behavior using that particular design. Simulations can be performed for each design of every iteration by using a call-back function in MATLAB, but this makes the problem computationally more expensive and it might even take few months for the algorithm to converge.

A solution that would not require simulations to be performed in the loop is to represent the system's behavior mathematically in an easiest form which will help to expedite this process. This required mathematical modeling of different design steps, semi-conductor loss calculation, MFT loss calculations etc. As already mentioned, the objectives of the optimization algorithm are

converter power loss and converter volume. So, mathematical models are required to obtain the values of these objective functions for every design in the iteration.

The MVDC collection of PV parks is not a conventional constant voltage or constant power application. So, optimizing the converter at a one particular operating point is not a good approach to efficiently leverage all the advantages of the topology. To overcome this, a test protocol adopted by California Energy Commission (CEC) which was originally developed by Sandia National Laboratories for grid tied inverters as a function of input DC voltage and output AC power is considered. According to this protocol, any inverter which requires a CEC approval have to be tested for efficiency at six different power levels and three different voltages and the weighted average efficiency is considered to rate the inverter [20]. Instead of considering a single operating point to optimize, the power losses of the converter are calculated at six different power levels and three different voltages and their weighted average is optimized. So, the objective power-losses of the optimization algorithm is replaced by CEC power losses. Different power levels and their corresponding weights that were considered for the analysis are mentioned in Table 1 [20].

Table 1: Weighting factors of different power levels defined by CEC

Output power	Weights
10%	0.04
20%	0.05
30%	0.12
50%	0.21
75%	0.53
100%	0.05

Power loss at all the six power levels must be obtained at three different voltage levels, $V_{in_{min}}$, $V_{in_{nom}}$ and $V_{in_{max}}$. For the MPPT voltage variation and its temperature dependency a string inverter solution Context CL125 from Schneider Electric is considered, $V_{in_{min}}$ and $V_{in_{max}}$ are calculated based on the method reported in their application note [21]. The analysis is based on series and parallel combination of a standard 6 inch, 315W poly-crystalline panel. The $V_{in_{min}}$ and $V_{in_{max}}$ are the MPP voltages calculated at -10°C and 50°C and are 970V and 1160V.

The second objective is to optimize the converter's volume. Due to the availability, the semi-conductor devices and the configuration of primary inverter and secondary rectifier are predefined. More details about the devices under consideration are presented in hardware implementation section. As already discussed, a full-bridge inverter on the primary side and a half-bridge rectifier on the secondary side are fixed and the same are used for further analysis. Since the semi-conductors are fixed, their corresponding volume is also fixed. Thus, the second objective of the optimization algorithm is to minimize the MFT volume since the series and parallel inductors L_r and L_m are considered to be integrated in the MFT as its leakage and magnetizing inductances.

To evaluate the objectives for every design in an iteration, the optimization algorithm would require mathematical representation of them. The MFT volume is a simple and straightforward calculation. CEC losses for every design is a sum of semi-conductor losses (sum of switching and conduction losses) and MFT losses (sum of core and conduction losses). This would require the mathematical representation of different losses as a function of the operating point.

3.2.1 Structure of the optimization algorithm

Before discussing the mathematical modeling of various parameters of the converter, it is important to understand the structure of the optimization algorithm. The algorithm has two important functions: fitnessFunction – this function returns the values of the objectives for every iteration and constraint function – this function holds and verifies if all the designs under consideration satisfy the user defined constraints or not. As discussed earlier, there are many variables in an LLC resonant converter that need a justified choice. These variables are divided into two categories: free variables and dependent variables. Free variables are those which are independently varied by the algorithm and dependent variables are calculated as a function of free variables and converter specifications for every iteration. A database of three different ferrite materials (3C90, 3C91 & 3C94) from Ferroxcube are considered for the algorithm to choose from. Since the intent was to develop an initial prototype from the core shapes readily available in the market, stacking of U cores is considered to obtain EE MFT core shape. Litz wire is considered to realize the primary and secondary windings of the MFT as this a high operating frequency application and using litz wire helps overcome the disadvantages of a magnet wire wound transformer. The free variables considered in this work are

$$X = [\ f_o\ L_n\ L_r\ W_c\ N_c\ CM\ N_p\ J_p\ d_1\ J_s\ d_2\ K_{dc}\ H_w\ K_{ww}\ ] \qquad\qquad 3.1$$

W_c is the width of the core, N_c is the no. of cores stacked, CM is the core material, N_p is no. of turns in the primary winding, J_p is the current density in primary winding, d_1 is the strand diameter of the primary winding, J_s is the current density in secondary winding, d_2 is the strand diameter of the secondary winding, K_{dc} is the ratio of core depth to its width, H_w is the height of the window and K_{ww} is the ratio of window width to its height. Figure 7 gives an overview of how the

optimization algorithm is organized. Along with the free variables and material database, the algorithm needs the converter specifications like nominal, min. and max. input voltages, CEC power levels and corresponding weights, transformer turns ratio, ambient temperature (T_a) and output voltage (V_o). The free variables must always be accompanied by their lower and upper bounds between which they can be varied by the algorithm. For every design under consideration, the algorithm checks if all the user defined constraints are satisfied and only then, the objectives are calculated for that design. If a design violates any of the constraints, the algorithm discards that design and moves to next iteration. The constraints that were considered in this work were Junction temperature of primary & secondary semi-conductor devices, temperature of MFT core and its windings, B_{max} in the core, required window width and range of the operating frequency. Upon satisfying the constraints, the dependent variables like the MFT geometry, resonant tank parameters etc., are calculated using the set of free variables and the user defined converter specifications. The resonant tank parameter calculation is performed using the method that was discussed in section 2.4. The core material parameters are obtained based on the choice of the algorithm for that iteration. Using the converter specifications, the max. values of currents flowing through the primary and secondary windings of the MFT are calculated which will then be used to calculate the no. of strands in both the windings (current densities & strand diameters which are the free variables will be used for this calculation). The semi-conductor losses and MFT losses are evaluated for different CEC output power levels. MFT volume is calculated. The algorithm uses the CEC power losses and MFT volume to make the decision whether the design must be saved until further analysis is done or it should be discarded. Mathematical modeling of various converter parameters, power losses etc., will be discussed in the next sub-section.
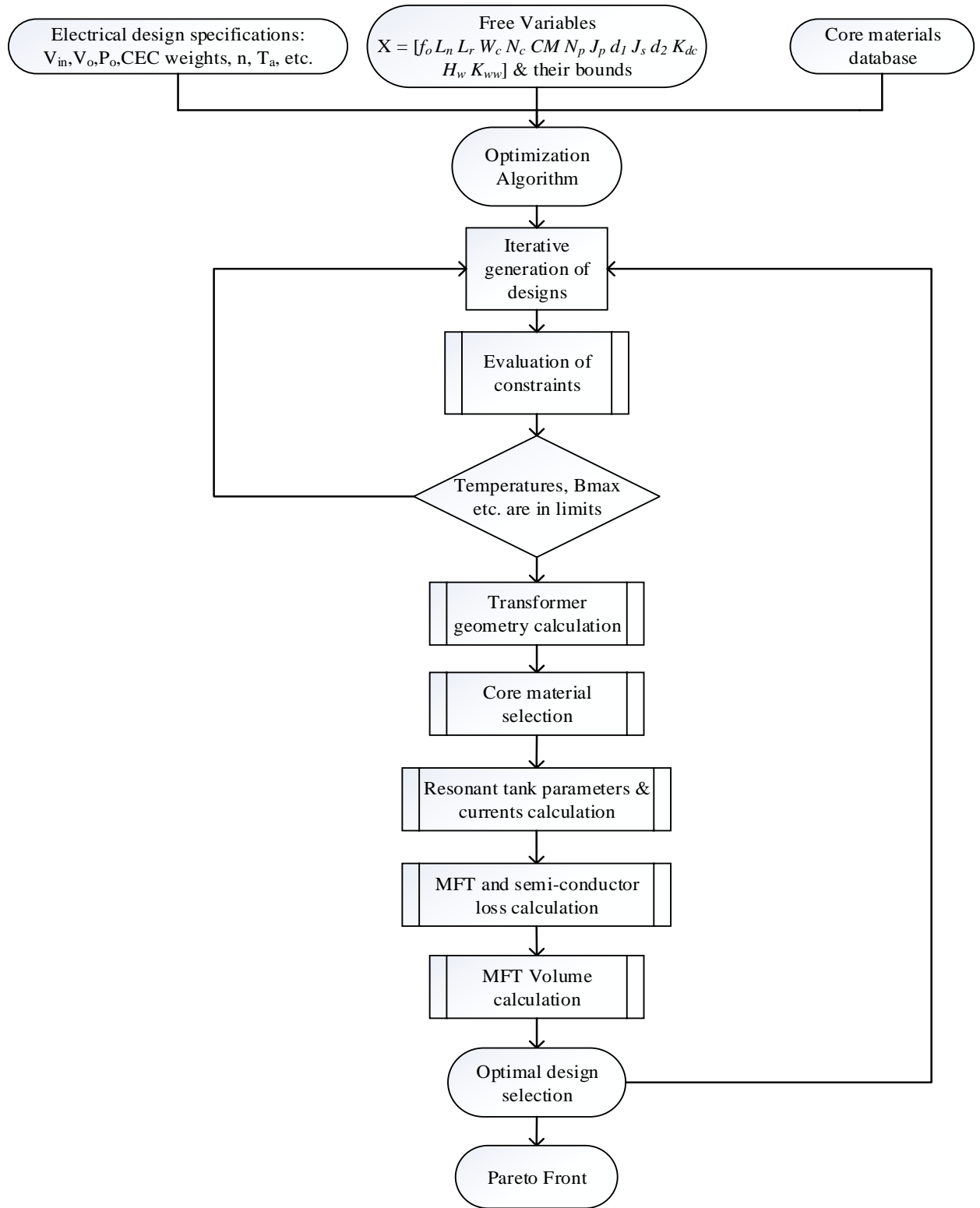
Figure 7: Overview of optimization algorithm

3.2.2 Mathematical modeling

The optimization algorithm can be used to perform co-simulations in the loop but that would make the optimization process computationally expensive and time to perform it would significantly be high. Alternatively, the same system behavior can be analyzed without simulations provided one can represent the behavior of different parts of the converter mathematically. The approach under discussion is something similar. The objectives CEC losses & MFT volume are calculated with the help of various mathematical models that will be discussed in this section.

RMS Current through the resonant tank:

Based on the FHA analysis that was discussed in section 2.3, the fundamental component of the applied voltage is considered to obtain the RMS value of current that is flowing through the resonant tank. Since the parallel inductor L_m is a part of the transformer, the current that is flowing through the series inductor L_r will flow though the MFT primary winding. As a result of this, there is only one unique value of current that has to be calculated which can help evaluate both the semi-conductor losses and MFT copper losses. The AC equivalent circuit which can be referred from Figure 5 is used to obtain the impedance offered by the converter (Z) at different operating points.

$$Z = \sqrt{\left(\frac{R_{ac}\omega^2 L_m^2}{R_{ac}^2 + (\omega L_m)^2}\right)^2 + \left(\left(\frac{R_{ac}^2 \omega L_m}{R_{ac}^2 + (\omega L_m)^2}\right) + \left(\frac{L_r C_r \omega^2 - 1}{\omega C_r}\right)\right)^2} \qquad 3.2$$

Using the gain function from equation 2.4, the switching frequency and corresponding R_{ac} can be found for different operating points defined by the CEC protocol. RMS value of the input current ($I_{P_{rms}}$) can be calculated using input voltage (V_{in}) and Z.

$$I_{p_{rms}} = \frac{4V_{in}}{\pi Z \sqrt{2}} \qquad\qquad 3.3$$

$I_{p_{rms}}$ and n can be used to calculate the value of secondary RMS current ($I_{s_{rms}}$) of the MFT. When it comes to accuracy, the FHA based RMS current model is not as accurate as a time domain based current model. But it is a good tradeoff between accuracy and computational complexity. [22] gives a good overview of time domain-based analysis of different operating modes and the respective parametric analysis.

Winding parameters:

Using the value of max. current flowing through the windings, current densities and strand diameters chosen by the algorithm, the number of strands in both the windings is calculated. Based on the user input on max. no. of strands, the algorithm can also come up with a parallel winding configuration if required without violating the available window area. The algorithm then evaluates the geometry of the windings and in cases where the winding cannot be accommodated in the available window height, multi-layer winding is also considered as a design alternative.

The geometry and configuration of the MFT windings are used to calculate the DC and AC resistances of both the windings. Copper losses in the primary and secondary windings of the MFT are function of the RMS current flowing through them and the AC resistance of the windings.

Core losses in the Medium Frequency Transformer:

The core volume of the MFT is calculated as a function of its geometrical free variables. Improved generalized steinmetz equation is used to obtain the core losses which is a function of core geometry, material, and converter operating parameters.

$$P_c = 2k_i f^\alpha B_m^\beta (0.5)^{1-\alpha} \qquad\qquad 3.4$$

And

$$k_i = \frac{k}{2^{\beta-1}\pi^{\alpha-1}\left(1.1044 + \frac{6.8244}{\alpha + 1.354}\right)}$$ 3.5

Where k, α and β are steinmetz coefficients and material dependent and P_c is the core loss per unit volume. The volume of the core calculated from the MFT geometry when multiplied gives the total core loss of the MFT for that operating point.

Semi-conductor loss evaluation:

The objective of the work is to design an LLC converter for MVDC collection of PV parks that can leverage all the advantages offered by an LLC configuration. As already discussed in previous sections, it is possible to achieve ZVS turn on of the low voltage devices and synchronous rectification of MV devices. The same is considered when evaluating the semi-conductor losses by the algorithm. Even though the switching frequencies are very high in this converter, both the LV and MV devices switch when current through the device is very close to zero. So, the turn OFF losses in the devices are fairly small compared to the output power. With zero turn ON losses and negligible turn OFF losses, the algorithm is only left with evaluation of the conduction losses of the semi-conductor devices.

The LV side inverter is realized using 1.7kV SiC FETs (C2M0045170P) from Wolfspeed and MV rectifier using 10kV Gen-3 SiC half-bridge module from Cree. A resistive based thermal network is used to calculate the steady-state temperature rise in both the devices. The temperature rise is used along with the temperature dependent conduction loss model of the device to calculate the device conduction loss. The loss data of the LV device is provided by the manufacturer but since the MV module is not commercially available, there is no data about the device

characteristics provided by the manufacturer. With the help of Double Pulse Test (DPT), the dynamic characteristics of the MV device are obtained. Various tests are performed at different test condition and energy losses (E_{on} & E_{off}) are calculated during the turn on and turn off transients. Optimum values of gate-voltage, turn ON and turn OFF resistances are chosen based on the observations from dynamic characterization. Static characterization is performed at different temperature and output characteristics of the device are obtained. Temperature dependent ON-state resistance models of the LV and MV devices are as follows

$$R_{ds_{pri}} = 0.041368 + (0.1611e - 3)T_{j_{pri}} + (0.0011e - 3)T_{j_{pri}}^2 \qquad 3.6$$

$$R_{ds_{sec}} = 0.2908 + (6e - 4)T_{j_{sec}} + (1e - 5)T_{j_{sec}}^2 \qquad 3.7$$

Where $R_{ds_{pri}}$ and $R_{ds_{sec}}$ are ON-state resistances of primary and secondary devices and $T_{j_{pri}}$ and $T_{j_{sec}}$ are their respective junction temperatures. These models are used to obtain the steady state conduction losses and the rise in the junction temperatures of the semi-conductor devices which is a design constraint.

Magnetizing and leakage inductances:

In a high frequency application, the estimation of leakage inductance is not a straightforward task. In applications like LLC resonant converters where part of or total series resonant inductor is being realized using the transformer's leakage inductance, the estimation of leakage inductance of the MFT should be as accurate as possible. A hybrid leakage inductance model is proposed in [23] which is based on Dowell's frequency dependent leakage inductance estimation [24]. The leakage inductance model proposed in [23] is for a simple MFT with single layer litz wire windings. The optimization approach proposed in this work is designed to explore most of the design space which includes parallel and multi-layer windings. So appropriate changes

are made to the model discussed in [23] so that it can be used for different types of winding configurations. The MFT's leakage inductance can be estimated from

$$L_\sigma = \frac{N_p^2 \mu_o L_w}{h_{eq}} \left[\frac{d_1 m_1}{3} F_1 + \frac{d_2 m_2}{3} F_2 + d_{iso} + d_{1_i} \frac{(m_1 - 1)(2m_1 - 1)}{6m_1} \right.$$
$$\left. + d_{2_i} \frac{(m_2 - 1)(2m_2 - 1)}{6m_2} \right]$$

3.8

And

$$F = \frac{1}{2m^2 \Delta} \left[(4m^2 - 1) \frac{\sinh 2\Delta - \sin 2\Delta}{\cosh 2\Delta - \cos 2\Delta} - 2(m^2 - 1) \frac{\sinh \Delta - \sin \Delta}{\cosh \Delta - \cos \Delta} \right] \qquad 3.9$$

Where N_p is the no. of primary winding turns, L_w is the mean turn length, d_1 and d_2 are the strand diameters of the primary and secondary windings, m_1 and m_2 are no. of equivalent foil layers in primary and secondary windings, d_{iso} is the isolation distance between the primary and secondary windings, d_{1_i} and d_{2_i} are twice the insulation thicknesses of the primary and secondary litz wire strands. The series resonant inductance L_r is a free variable in this optimization approach. The leakage inductance model presented in equation 3.8 can be used by the algorithm to know if estimated leakage based on a fixed d_{iso} is equal to the required L_r or the d_{iso} can be found for the desired leakage. On the other hand, the parallel resonant inductance L_m is a derived or dependent parameter obtained from L_n and L_r and is a unique value for each design. Since the parallel resonant inductor is being realized as the magnetizing inductance of the MFT, the magnetizing inductance model can be used to derive the air gap required to achieve the L_m.

$$L_m = \frac{\mu_o N_p^2 A_c}{d_{ag}} \qquad 3.10$$

Where A_c is the area of cross-section of the MFT core and d_{ag} is the air gap required to obtain a specific value of L_m.

3.3   Performing the Optimization

Lower and upper bounds of the free variables had to be wisely chosen to explore most of the search space that is being targeted. In the early stages of developing this optimization algorithm, series inductance L_r was not a free variable and was being derived from other dependent variables. Since for the same L_n, both the inductances were derived parameters, the population of designs on the pareto front was not uniformly distributed as expected. Choosing from such concentrated population does not give the designer the flexibility needed to choose a design from. Another approach that had to change was realizing the series inductor using MFT's leakage inductance. The L_r was assumed to be equal to MFT's leakage inductance and this assumption was being used to derive the isolation distance required to achieve a specific leakage. This resulted in a scenario where the design space was confined to a very small region and the converter's performance is also not very satisfactory for these designs. To overcome this, the L_r has been made a free variable. Designs even with leakage lower than L_r are considered since part of the L_r can be leakage and the remaining inductance required can be achieved by an external inductor. The pareto front obtained from the algorithm is presented in Figure 8. X-axis is CEC power losses in watts which was discussed in previous sections and Y-axis is the box volume of the MFT in Liters. The points in the pareto front are different designs with different CEC losses and volume. There are a wide range of optimal designs to choose from. From very low volume and high losses to very high volume and lower losses, an ideal choice would be choosing a design closer to origin because of its balance between losses and volume.
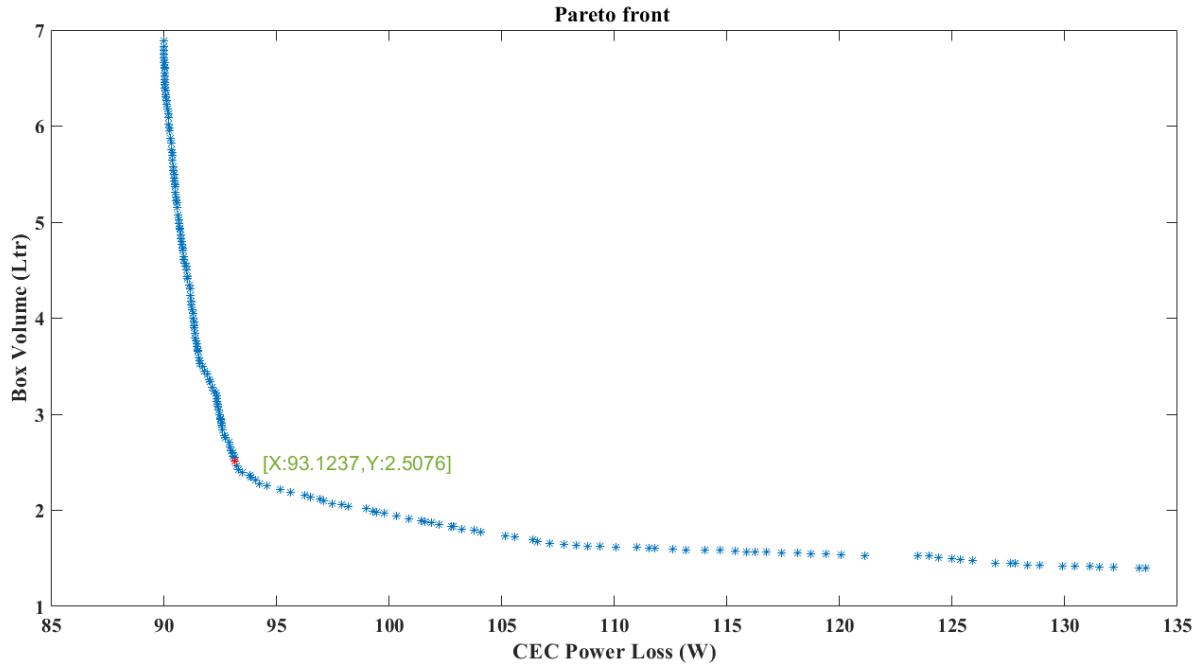
Figure 8: Pareto optimal solutions

But when it comes to prototyping, this choice is affected by many parameters mostly materialistic. The choice of the design in this work is based on the availability of closest possible materials like MFT cores, litz wire etc. The design chosen has a CEC power loss of 93.1237W and volume 2.5076 ltr. Free variables of this design can be referred from Table 2.

Table 2: Free variables of the design chosen

Free Variables			
Variable	**Value**	**Variable**	**Value**
f_o	76812 Hz	J_p	3.688 A/mm^2
L_n	6	d_l	40.9 μm
L_r	185.915 μH	J_s	4.189 A/mm^2

W_c	23.1198 mm	d_2	38 μm
N_c	4	K_{dc}	0.648
CM	3C94	H_w	57.556 mm
N_p	22	K_{ww}	1.391337

The dependent or derived variables like resonant tank parameters etc. are tabulated in Table 3.

Table 3: Derived converter parameters

L_m	1.1 mH	C_r	23.092 nF
A_c	2771 mm^2	N_s	67

The CEC efficiency of the selected design is 99.4%. Loss distribution of the converter at different power levels and nominal input voltage are plotted which can be referred from Figure 9.
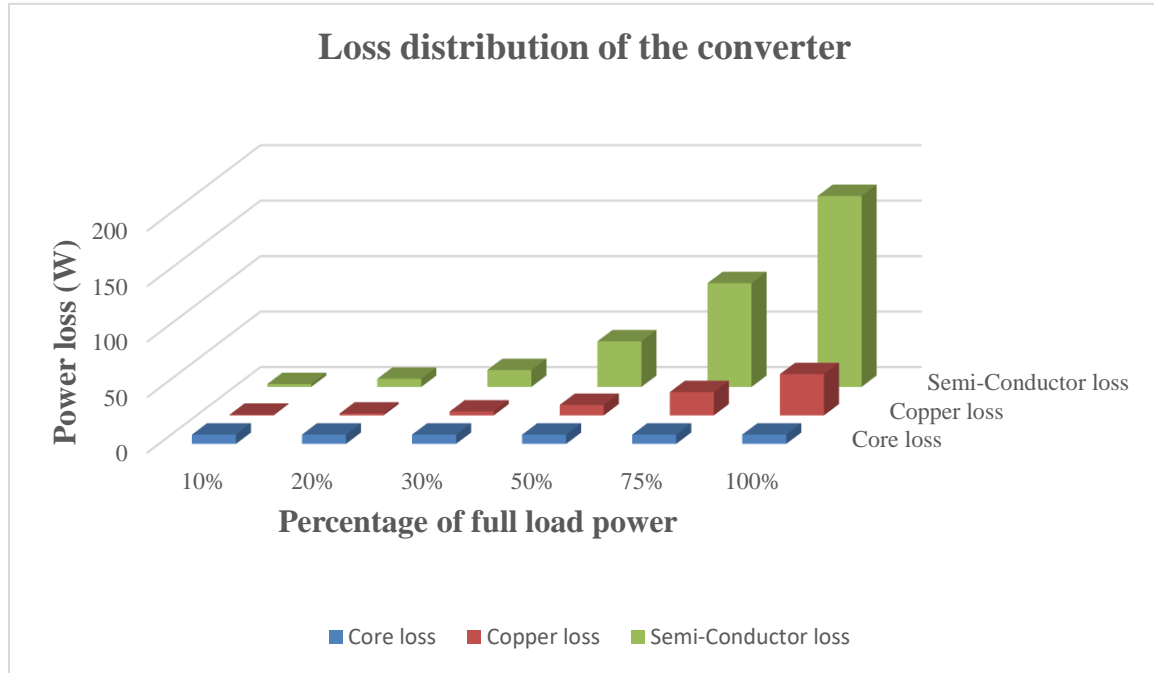

Figure 9: Loss distribution at different output power levels

The hardware implementation of this design will be discussed in detailed in the next chapter.

CHAPTER 4

HARDWARE IMPLEMENTATION

4.1   Overview

A pareto front consisting of optimal designs was obtained and a design was chosen which is a tradeoff between the CEC losses and MFT volume. The design that was selected is marked in red in Figure 8. The derived converter parameters, analysis conditions and estimated performance of the selected design were discussed in previous chapter. This chapter is a detailed discussion of the fabrication and testing of initial prototype. This involves component selection, steps followed in fabrication and tests conducted along with the discussion on results obtained. The first step in the prototype development was to build the LV and MV power electronic modules and to test them individually to their full capacity. Once the power electronic modules are developed, the next step is to get the MFT fabricated, characterize, and test the MFT to its full capacity. The prototype that is built to validate the analysis is slightly different from the selected design due to various reasons that will be discussed further in this chapter.

4.2   Component Selection

The first fixed parameter that was also considered as an input to the optimization was choice of semi-conductor devices. A 1.7kV, 72A SiC MOSFET C2M0045170P from Wolfspeed is used to develop the primary LV inverter. Detailed datasheet and development models for this device can be found from their webpage [25]. The thermal and loss models for this device were available from the manufacturer which were used to evaluate the temperature rise and losses at various operating points in the optimization algorithm. The MV half bridge rectifier is realized

using a 10kV gen-3 XHV SiC half bridge module from Cree. Since this is not a commercially available device, the device characteristics were not provided by the manufacturer. So, the secondary power electronics module was initially built before anything else in the converter and was used to perform Double Pulse Test (DPT). Using DPT, the dynamic characterization of the device was performed extensively to determine the device characteristics and also an optimal turn ON and turn OFF resistance value. Static characterization was also performed to determine the output characteristics at different temperatures.

From all the commercially available ferrite shapes of 3C94 materials, it was difficult to obtain the exact match of required area of cross-section of the MFT core. Different shapes and stacking combinations were considered. A U core U93/76/30 from Ferroxcube [26] is used as the base element to realize the MFT core geometry. Two U cores are stacked to form an equivalent E core and two E cores to form the MFT core geometry. Two of such combinations are stacked to achieve the required depth of the MFT core.

Due to unavailability of the exact match of the litz wire profile from the selected design, the closest litz wire available was chosen keeping the area of cross-section of copper fixed. A 38-strand gauge litz wire with 2500 strands was used to fabricate the primary winding and a 44-strand gauge, 1500 strands litz wire was used for the secondary winding. Both the litz wires have a circular profile unlike the square profile that was considered for the analysis in the optimization. A resistive load was fabricated to dissipate the power delivered by the converter. The resistive load bank is a combination of 108 wire wound resistors connected in different series and parallel configurations which can dissipate up to 20kW at 7kV.

4.3   Fabrication of different hardware stages

As discussed earlier, the first step was to fabricate the MV power electronic block, characterize the device and use the data obtained as an input to the optimization algorithm for further analysis. The MV block consists of five boards: a main power board, two gate driver boards and two gate driver power supplies one for each device. The boards were designed using Altium designer.
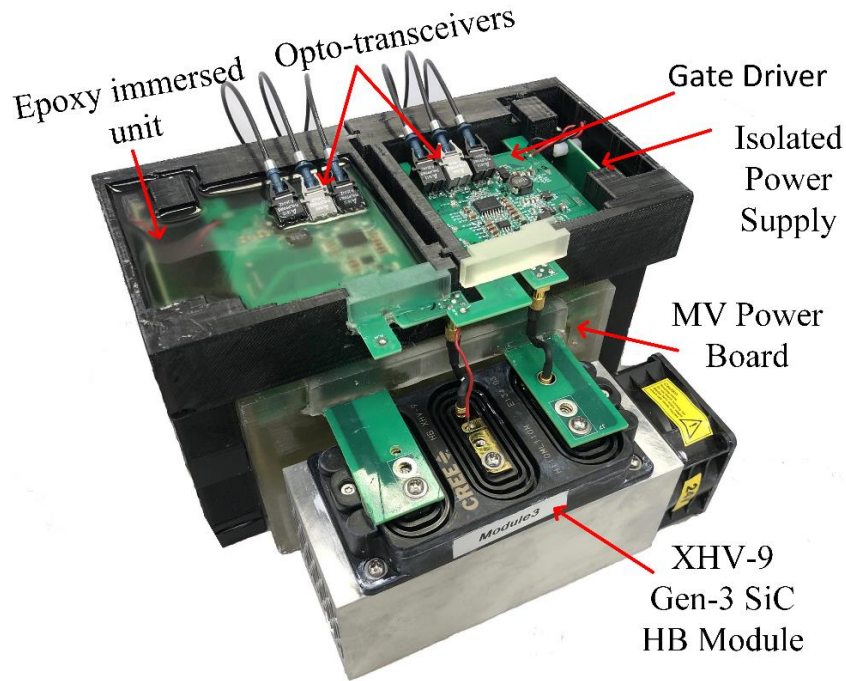

Figure 10: MV Power Electronics block

An overview of different components in the MV block can be obtained from Figure 10. The power board also accommodates six 4.5 µF capacitors in series whose mid-point is connected to one of the MFT secondary winding terminals. To achieve higher power densities, the power and gate driver boards have to be placed as close to each other as possible. But, due to MV operation, the required isolation level is very high to meet the industry standards. To increase the isolation

level and to make the setup very compact, all the MV boards (power, gate driver and power supply boards) are immersed in epoxy. The communications for control and feedback with the MV block are implemented using opto-transceivers as there are no commercially available ICs available with the required isolation levels. The opto-transceivers are connected to the signal processing & controls board which is a part of the LV power electronics block using fiber optic cables. The power board is individually potted from gate driver and power supplies using 3D printed boxes to contain them. The boards are placed in the boxes, filled with epoxy, and cured using a vacuum oven. MV block is 218×109 ×140mm without the HB module & heatsink and 218×200 ×140mm all together. Box volume of the MV power electronics module is 6.1 Ltr.

The LV power electronics block is slightly simpler in construction with two PCBs as shown in Figure 11.
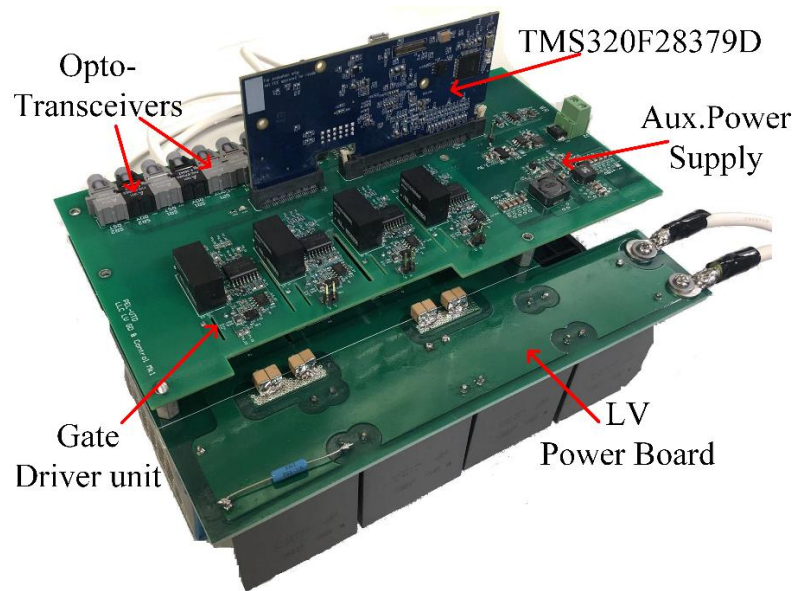

Figure 11: LV Power Electronics Block

The power board has four C2M0045170P MOSFETs, input DC bus capacitors and an output current sensor. The power board is mounted on the heatsink in such a way that the

MOSFETs are between the board and the heatsink. This will ensure that most of the heat from the MOSFETs is drawn out from the case and into the heatsink. The LV gate driver and controls board sits above the power board. This board has components to control the entire converter. The auxiliary power supplies provide low voltage supply to microcontroller (MCU), gate driver ICs, isolated DC-DC converters of the gate driving circuits, signal conditioning circuits, sensors etc. The MCU which is being used in this prototype is TMS320F28379D from C2000 family of Texas Instruments. Different peripherals of MCU that are being used by this prototype are EPWMs to provide PWM signals to LV and MV devices, GPIOs to control the logical circuits, SPI to obtain output voltage feedback, ADCs to obtain on board feedbacks, COMPs for real-time current monitoring and also for added protection, and TZ for fault protection. This board also accommodates opto-transceivers to drive the MV side devices and to obtain output voltage feedback. The dimensions of the LV block are 210×170 ×140 mm and its box volume is 4.998 Ltr. To validate the controls and to obtain an optimal gate resistance for the LV device, various tests have been performed on the LV block. Test results from one such test at 900V input and 12.5kW output and using the LV block in inverter operation is shown in Figure 12. The power 12.5kW was being circulated through an inductor during which the inductor losses were104W. The losses in the LV converter were 49W at which point the LV block was operating at an efficiency of 99.61%. All the boards in LV and MV blocks were fabricated and tested in house and as many tests as possible were conducted to make sure there are not too many variables that can cause a failure during the full converter test. The current sensor that is used to measure the output current of the LV block is CMS3100 from Sensitec. A Current Transformer (CT) 2878 from Pearson is used to monitor the secondary current of the MFT. The output of both the current monitors is processed

by differential conditioning circuits and fed to the MCU. The feedback of the input voltage is obtained using a resistive divider.
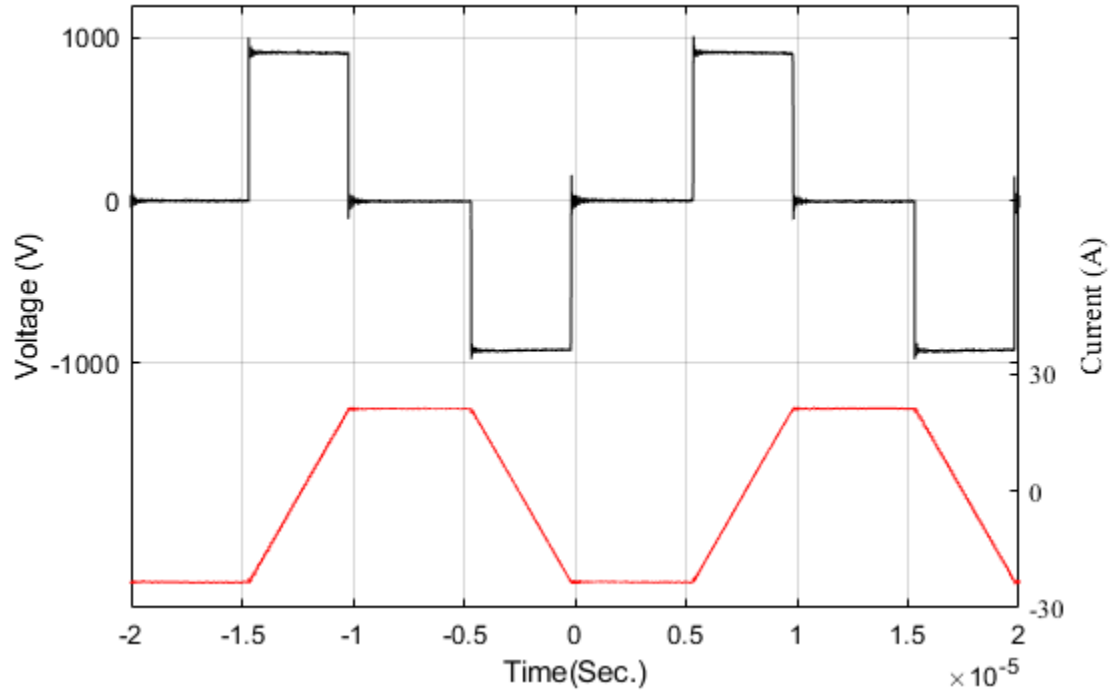

Figure 12: LV block output in inverter operation with D < 0.5

With both the power electronic blocks fabricated, the next step is to fabricate the MFT. The core that was selected was already discussed in the previous sub-section. Four U cores are used to realize an EE transformer core profile and two such combinations are stacked next to each other to achieve the required area of cross-section. So, eight U cores are used for the fabrication of this MFT. With min. required clearances from the core in all directions, bobbins are 3D modeled for both the windings to make sure the windings would fit exactly where they must be placed. The primary winding of the MFT is a simple single layer winding with a 2500-strand litz wire. The secondary winding is a three-layer, sectionalized winding where the winding is divided into three sections and each section has three layers of MFT secondary winding. The MFT is designed to

also accommodate spacers between each layer of winding which will allow the air circulation in case forced air cooling is required.
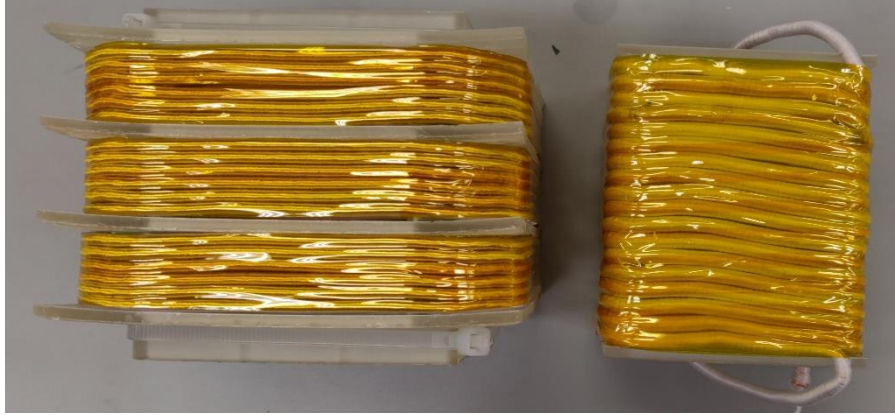

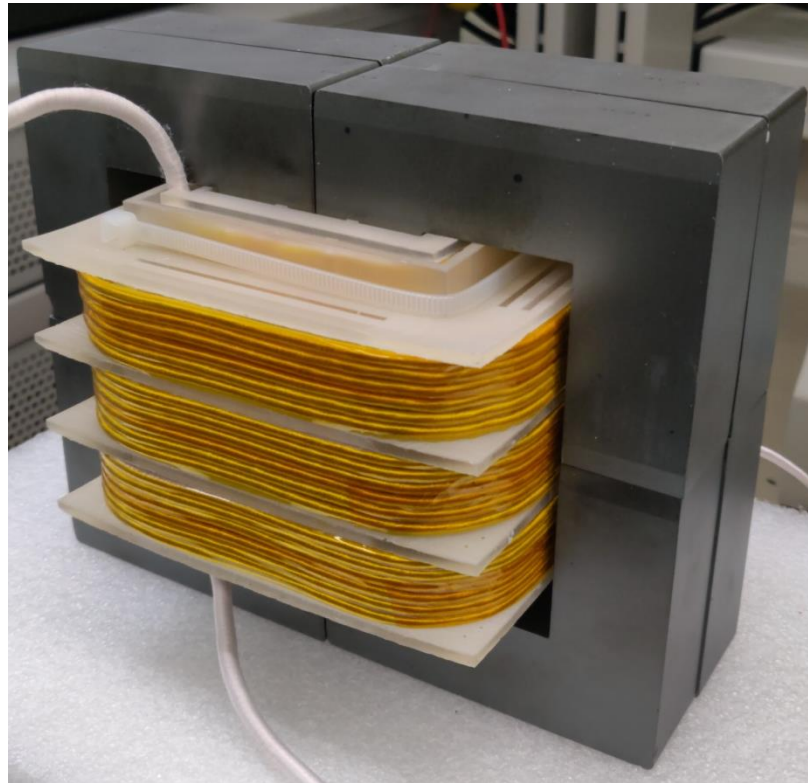
Figure 13: Secondary & Primary windings of the MFT

Figure 14: MFT before winding impregnation
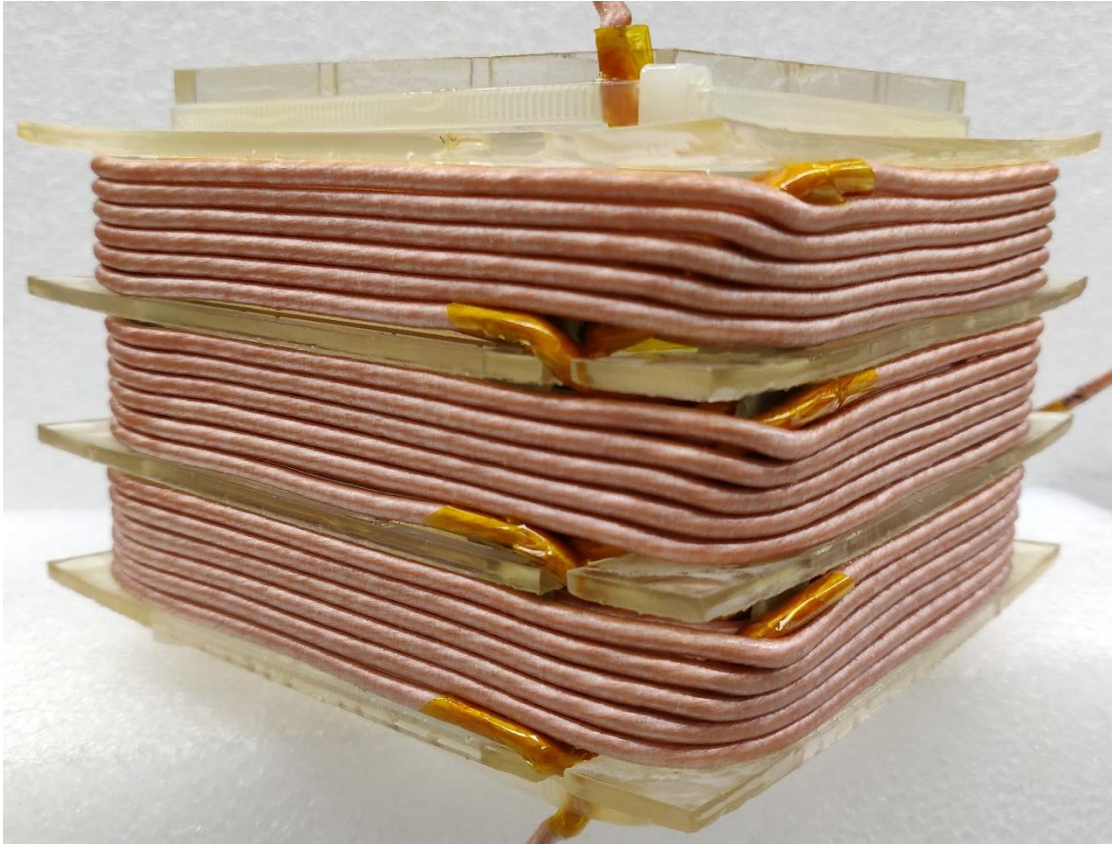
Figure 15: Secondary winding after impregnation

The sectionalized winding is chosen for the MFT secondary winding to reduce the parasitic capacitance associated with the MFT. The bobbins were fabricated using a 3D printer inhouse. An SLA type 3D printer Form2 from Formlabs is used for all the 3D printed structures required for the prototype at different stages.

Finished windings on their respective bobbins are shown in Figure 13. The windings would still have to go through the impregnation process which improves the insulation strength of the windings and prevents any dielectric breakdown. Figure 14 shows the initial version of MFT put together for a winding fit check and to verify the dimensions like clearances, isolation distance between the windings etc. The windings are then impregnated at 80°C and made ready for the final

assembly. An impregnated assembly ready secondary winding is shown in Figure 15. After the windings were impregnated, the MFT was assembled and its parameters winding resistances, leakage and magnetizing inductances were measured using an impedance analyzer. The next step was to perform a Hipot-test on the MFT. Hipot test was performed up to 7kV for a duration of one minute which the MFT passed. The dimensions of the assembled MFT are 186×127×152 mm with a volume of 3.5905 Ltr. The assembled converter is shown in Figure 16.
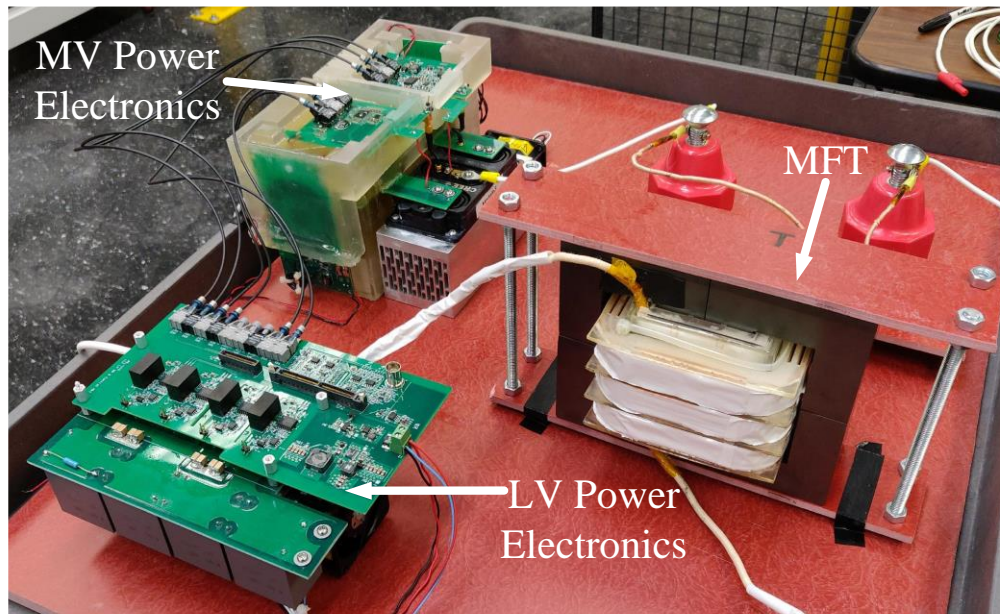
Figure 16: Final assembly of the converter

Table 4: Parameters of the prototype

Prototype Parameters					
Variable	**Value**	**Variable**	**Value**	**Variable**	**Value**
f_o	76812 Hz	J_p	1.506 A/mm^2	L_m	1.325 mH
L_n	6	d_1	100.7 μm	A_c	3408 mm^2
L_r	24.465 μH	J_s	2.759 A/mm^2	C_r	0.18 μF

W_c	28.4 mm	d_2	50.2 μm	N_s	54
N_c	2	K_{dc}	1.056	n_1	2500
CM	3C94	H_w	48 mm	n_2	1500
N_p	17	K_{ww}	0.75417		

The parameters of the prototype are listed in Table 4. These parameters are different from that of the selected design because of the choices made in the prototyping. The geometry of the MFT core and the windings are different because the core geometry chosen is not an exact match to the required design. Change in the MFT core geometry also affects the winding geometry. Also, the secondary winding of the MFT in the prototype has a different construction as sectionalizing and spacers were introduced between each layer. Though the MFT's leakage in the design offers only part of the required L_r, the leakage of the MFT prototype is significantly different from the estimated value because:

- The isolation distance between the primary and secondary windings is designed to be 10mm but because the radius at the corners of the bobbin is significantly small compared to the min. radius at which the litz wire could be bent at right angles, this distance came down to 3 - 4mm.

- Introduction of spacers and sectionalizing the winding

- Also, since both the windings are hand wound, the accuracy to achieve the exact design dimensionally is significantly low.

The selected design could still be achieved in terms of obtaining the same resonant tank parameters by adding an external series inductor and changing the resonant capacitor to the

required value. But for initial tests, the converter is to be extensively tested at nominal input voltage and different loads to validate the entire analysis based on the results that will be obtained.

The tests are conducted in an isolated high voltage cage where all the units under test will be inside the cage which have to be controlled remotely from outside. A 30kW DC power supply unit from Magna is used as an input to the converter. The MCU is always run in a debug mode during all the tests to make sure that human intervention is possible to manually react to a fault. Due to unavailability of power measurement which can support the measurement of high frequency and high voltage signals, only an oscilloscope is used to record all the test data. The oscilloscope is also placed outside the cage for it to be accessible.

Figure 17: Test equipment arrangement

The arrangement of different test computer, different test equipment is shown in Figure 17. The test setup Figure 18 consists of primary DC power supply, converter, resistive load bank and auxiliary power supplies for heatsinks, gate driving etc.
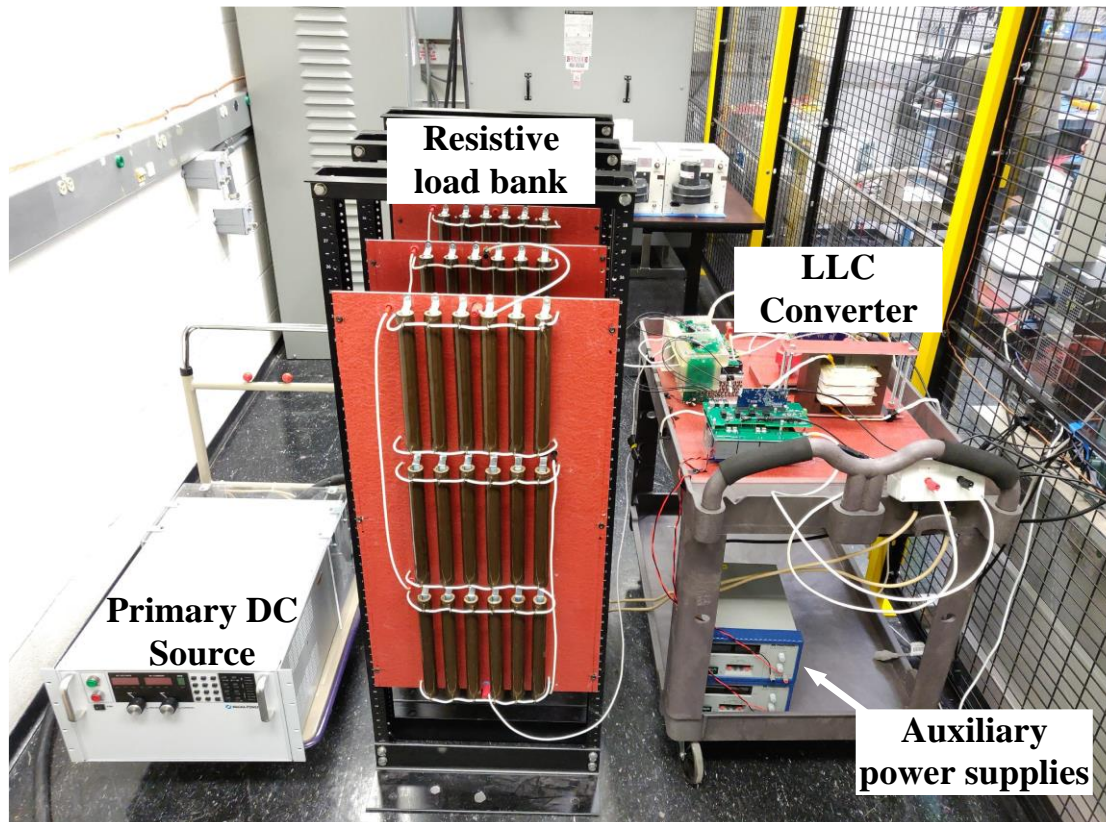
Figure 18: Converter test setup

4.4 Test Results

In the initial tests, the converter was tested at half the nominal input voltage, which is 550V, resonant frequency 76812Hz and with an output resistance of 2500Ω, 5kW of power was being dissipated in the load - Figure 19. At same frequency and nominal input voltage 1100V, the test was performed again dissipating 20.5kW in the load bank - Figure 20. The converter has an overall efficiency of 99.454% at this operating point whose input and output DC waveforms can be referred from Figure 21.

Figure 19: Inverter & MFT outputs at 550V input & 3.5kV, 5kW output

Figure 20: Inverter & MFT outputs at 1.1kV input & 7kV, 20.5kW output

Figure 21: Converter input 1.1kV and output 7kV at 20.5kW

CHAPTER 5

CONCLUSION
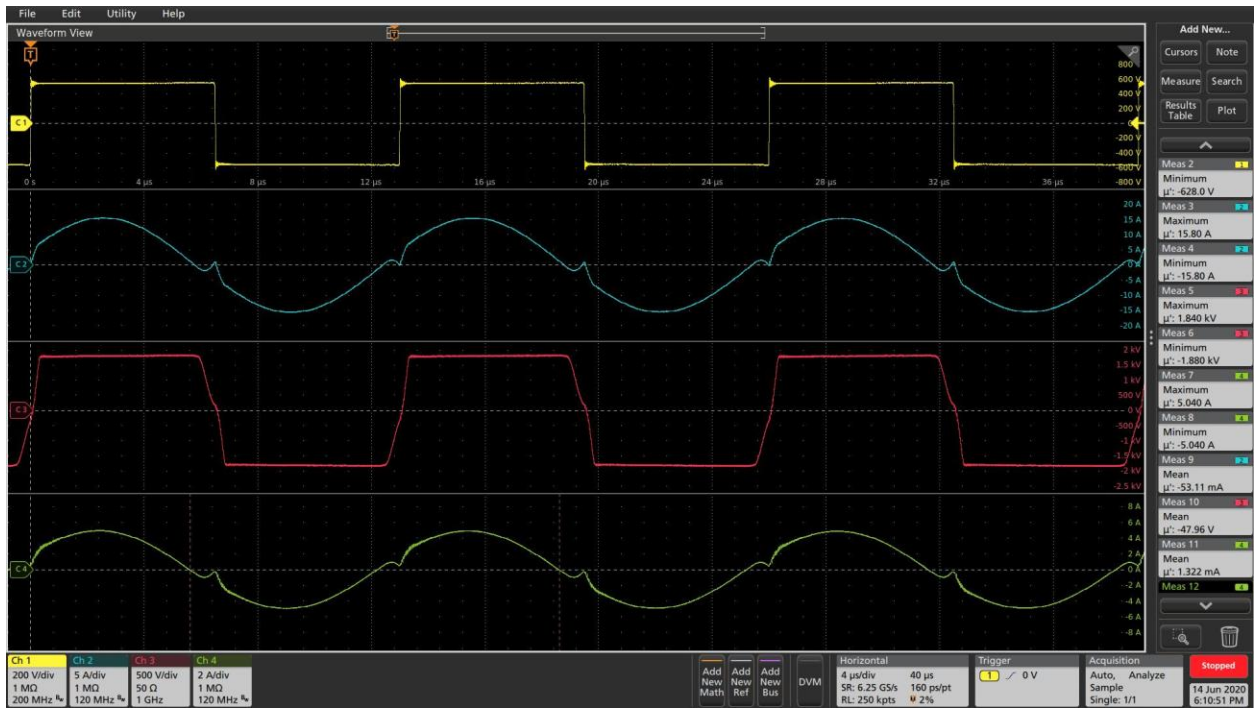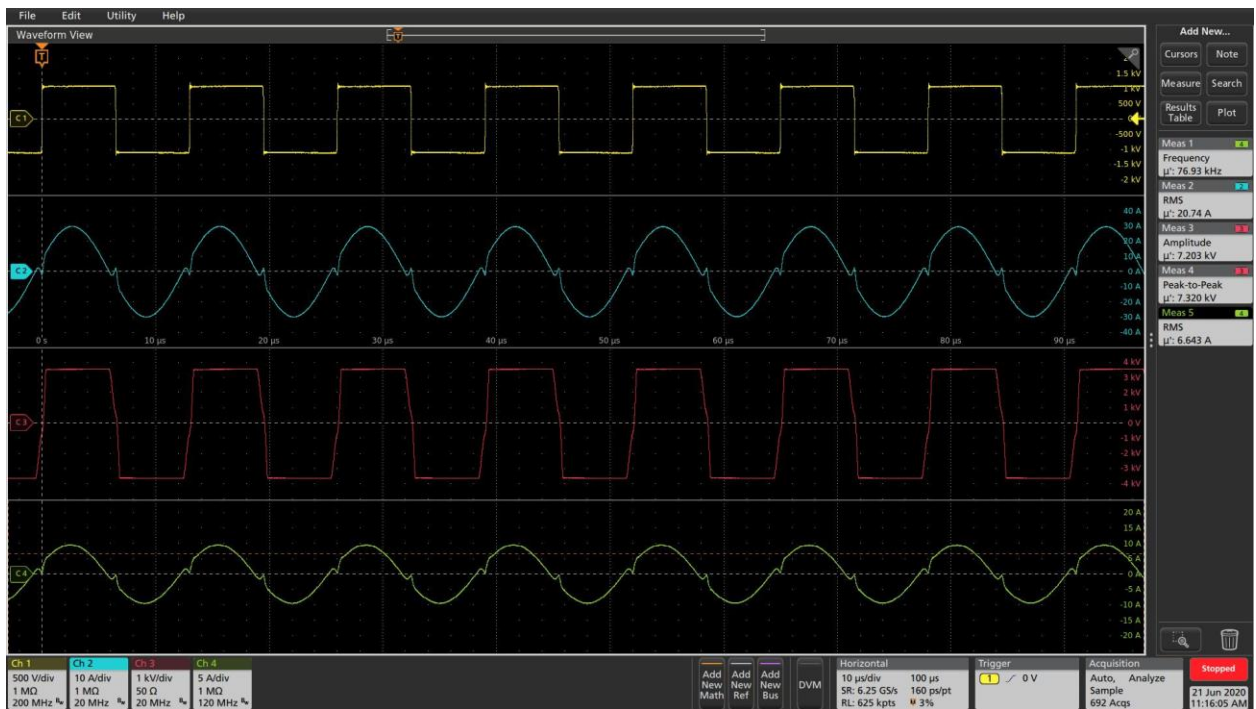
5.1   Summary and conclusions

Latest advancements in device technology especially in SiC devices have unlocked the potential to achieve higher efficiencies and higher power densities in many applications. PV integration being one of them, the use of SiC devices in such applications would bring many advantages to such systems. This work aims to reduce the LCOE in PV systems which were traditionally considered expensive alternatives for energy generation. Choosing an MVDC collection over conventional MVAC collection helps in many ways to reduce the capital in energy generation systems like PV, wind etc. Growing research efforts by researchers from all over the world are providing promising results and design alternatives using SiC devices. Industries like plug-in Electric Vehicles (EV) who already started using SiC in their products are proving the reliability and improved efficiencies by moving to SiC technology. This is encouraging for many other industries to unveil potential applications and come up with compact, efficient, and reliable power conversion systems. The cost of the devices is expected to significantly decrease faster than expected due to increased interests from industry giants.

This work is one such effort to come up with efficient, compact, and cost-effective architecture for collection of PV parks. An LLC resonant based isolated DC-DC converter configuration is proposed for MVDC collection of PV parks. The advantages of using the proposed configuration are discussed. An FHA based converter analysis and design procedure using the same is presented. A simulation-based approach to obtain an optimal design for the converter was discussed. The design variables and their significance are outlined and with no justified approach

for the choice of these variables, Multi-objective optimization is chosen to provide an optimal design that can help validate the advantages of the proposed configuration. A genetic algorithm available in MATLAB was used to perform the optimization. The structure of the optimization algorithm was presented, and mathematical models of different converter parameters were derived and explained in this work. The advantages and disadvantages of approximations made as a part of this work were explained. The optimization results are provided, and a design is selected for the proof of concept. Steps involved in fabrication of different stages of the converter are explained in detailed and the implications of design choices during prototyping were outlined. A 1.1/7 kV, 25kW isolated LLC resonant DC/DC converter was built and tested at nominal input voltage and 20.5kW output. An efficiency of 99.454% was achieved during this test and the prototype has a power density of 2.0419kW/L which is very close to the estimated power density 2.2043kW/L of the selected design. Box volume of the selected design was 13.6096L and that of the prototype is 14.6925L. The CEC efficiency of the selected design is 99.23% which is yet to be validated by the prototype. During the initial tests, the shape of the output current of the LV inverter was observed to be unusual in LLC resonant converters. Analysis is underway to identify the reason which could be one or both of: higher leakage inductance on the secondary winding of the MFT, significant output capacitance of the MV device. This requires further analysis.

5.2   Future Scope

The work opens up an opportunity to use LLC converters not only in MVDC collection architecture but in similar applications which require wide range of load and voltage regulation. The optimization algorithm was developed to be versatile to optimize an LLC converter design for any application with minimal to no changes. Improvements to this work: to start with, the FHA

analysis that was used to the converter modeling and design procedure can be replaced with more accurate approaches like time-domain analysis or an operation-mode based approach. This would only be helpful when the analysis is made simpler. The choice of semi-conductor devices can also be a design variable. Different configurations like half-bridge, full-bridge, series or paralleling of devices, multi-level converters etc., can be analyzed and the appropriate choice can be made for the application. The type of the MFT, different winding configurations and materials can be explored to make a right choice. The proposed converter is designed to inherently implement sub-field level MPPT but in uneven terrains, the MPPT voltage could be different for each string which might require a string pair level MPPT stage. So, a two-stage configuration can also be explored with different topology choices for the MPPT stage. In the two-stage approach, the resonant converter could be designed to operate at resonance to achieve highest efficiency and power density and all the voltage regulation can be handled by the MPPT stage. This would be an interesting analysis as there might be a tradeoff unlike what is expected where the voltage variation is divided between both the stages and one such design might be more efficient and compact.

REFERENCES

[1] N. Aspinall, L. Mills, D. Strahan, R. Boyle, V. Cuming, K. Stopforth, S. Heckler and L. Becker, "Global Trends in Renewable Energy Investment 2019," 2019.

[2] S. Lundberg, *Wind Farm Configuration and Energy Efficiency Studies - Series,* Ph.D. dissertation, Chalmers Univ. Technol.,G¨oteborg, Sweden, 2006.

[3] G. Stamatiou, K. Srivastava, M. Reza and P. Zanchetta, "Economics of DC wind collection grid as affected by cost of key components," in *World Renew. Energy Congr*, 2011.

[4] J. Yang, J. E. Fletcher and J. O'Reilly, "Multi-terminal DC wind farm collection and transmission system internal fault analysis," in *IEEE International Symposium on Industrial Electronics*, 2010.

[5] L. Zhang, K. Sun, Y. Xing, L. Feng and H. Ge, "A Modular Grid-Connected Photovoltaic Generation System Based on DC Bus," *IEEE Transactions on Power Electronics,* vol. 26, pp. 523-531, FEBRUARY 2011.

[6] H. A. B. Siddique, S. M. Ali and R. W. D. Doncker, "DC collector grid configurations for large photovoltaic parks," in *15th European Conference on Power Electronics and Applications (EPE)*, 2013.

[7] H. A. B. Siddique and R. W. D. Doncker, "Evaluation of DC Collector-Grid Configurations for Large Photovoltaic Parks," *IEEE TRANSACTIONS ON POWER DELIVERY,* vol. 33, FEBRUARY 2018.

[8] D. Chung, C. Davidson, K. A. R. Fu and R. Margolis, "U.s. photovoltaic prices and cost breakdowns: Q1 2015 benchmarks for residential, commercial, and utility-scale systems," Technical report : National Renewable Energy Laboratory, 2015.

[9] M. D. Bellar, T. S. Wu, A. Tchamdjou, J. Mahdavi and M. Ehsani, "A review of soft-switched DC-AC converters," *IEEE Transactions on Industry Applications,* vol. 34, pp. 847-860, 1998.

[10] Y. Chen, X. Wu, Z. Qian and W. Zhang, "Design and optimization of a wide output voltage range LED driver based on LLC resonant topology," in *8th International Conference on Power Electronics - ECCE Asia*, 2011.

[11] K. Jin, X. Ruan, M. Yang and M. Xu, "A Hybrid Fuel Cell Power System," *IEEE Transactions on Industrial Electronics,* vol. 56, pp. 1212-1222, 2009.

[12] Z. Liang, R. Guo, J. Li and A. Q. Huang, "A High-Efficiency PV Module-Integrated DC/DC Converter for PV Energy Harvest in FREEDM Systems," *IEEE Transactions on Power Electronics,* vol. 26, pp. 897-909, 2011.

[13] C. Chang and G. Bruning, "Voltage-fed half-bridge resonant converter for multiple lamp independent operation," in *IEEE Industry Applications Conference*, 2001.

[14] I. Batarseh, "Resonant Converter Topologies with Three and Four Energy Storage Elements," *IEEE Transactions on Power Electronics,* vol. 9, pp. 64-73, 1994.

[15] *An introduction to LLC resonant half-bridge converter,* ST Microelectronics, 2008.

[16] J. Lazar and R. Martinelli, "Steady-state analysis of the LLC series resonant converter," in *Annual IEEE Applied Power Electronics Conference and Exposition*, 2001.

[17] T. Duerbaum, "First harmonic approximation including design constraints," in *INTELEC-International Telecommunications Energy Conference*, San Francisco, CA, USA, 1998.

[18] R. L. Steigerwald, "A comparison of half-bridge resonant converter topologies," *IEEE Transactions on Power Electronics,* vol. 3, pp. 174-182, 1988.

[19] B. Lee, M. Kim, C. Kim, K. Park and G. Moon, "Analysis of LLC Resonant Converter considering effects of parasitic components," in *International Telecommunications Energy Conference, Incheon*, 2009.

[20] [Online]. Available: https://pvpmc.sandia.gov/modeling-steps/dc-to-ac-conversion/cec-inverter-test-protocol/.

[21] [Online]. Available: https://solar.schneider-electric.com/product/conext-cl125-string-inverter/.

[22] X. Fang, *Analysis And Design Optimization Of Resonant Dc-dc Converters,* 2012.

[23] M. Mogorovic, *Modeling and Design Optimization of Medium Frequency Transformers for Medium-Voltage High-Power Converters,* EPFL, 2019.

[24] P. L. Dowell, "Effects of eddy currents in transformer windings," *Institution of Electrical Engineers,* vol. 113, pp. 1387-1394, August 1966.

[25] Wolfspeed, [Online]. Available: https://www.wolfspeed.com/power/products/sic-mosfets/1700v-silicon-carbide-mosfets.

[26] FERROXCUBE, [Online]. Available: https://www.ferroxcube.com/upload/media/product/file/Pr_ds/U93_76_30_I93_28_30.pdf.

BIOGRAPHICAL SKETCH

Sai Kiran Voruganti was born in Miryalaguda, a small town in Telangana state, India. He received his bachelor's degree in Electrical & Electronics Engineering from CVR College of Engineering, Hyderabad, India in 2017. Between 2017-2018, he worked as a Graduate Engineer Trainee (Electrical Engineering) at Mitsubishi Elevators Ltd., and as Assistant Systems Engineer at Tata Consultancy Services Ltd., Hyderabad. His earlier works during his bachelor's degree include designing a solar inverter, an AC drive design using 2,3 and 5 level diode-clamped multi-level inverters. He joined the Power Electronics Lab at UTD, supervised by Dr. Ghanshyamsinh Gohil in 2018.There, he started working towards his thesis and participated in some other projects like a 30kVA SiC inverter for grid tied applications, a reconfigurable 30kW SiC based extreme fast charger for EVs, Conducted EMI reduction in Input Parallel & Output Parallel (IPOP) systems. His research interests are power conversion systems for EVs, renewables, battery charging, applications of machine learning and artificial intelligence to solve electrical and other engineering problems etc.

SAI KIRAN VORUGANTI

EDUCATION

M.S in Electrical Engineering   August 2018 to August 2020
The University of Texas at Dallas   CGPA: 3.67/4.0
B.Tech in Electrical and Electronics Engg.   May 2017
CVR College of Engg., Hyderabad, India   GPA: 3.3/4.0

SKILLS

MATLAB, SIMULINK, PLECS, PSIM, ANSYS, CCS, Altium Designer, SolidWorks, DipTrace, KiCAD, PSPICE, LTspice, C, 3D printing, well versed in using test & measurement equipment (Oscilloscope, Power analyzer etc.) and hardware tools.

RESEARCH & PROFESSIONAL EXPERIENCE
PUBLICATIONS

- *Common-mode Current Analysis and Cancellation Technique for Dual Active Bridge Converter based DC System*, ECCE-2019
- *Performance Evaluation of 10kV SiC-based Extreme Fast Charger for Electric Vehicles with Direct MV AC Grid Interconnection*, APEC-2020
- *SiC-Enabled Medium Voltage Isolated DC-DC Converter based Power Optimizer for Large Photovoltaic Parks,* APEC-2020

Power Electronics Intern in Linear Labs, LLC, Fort Worth, TX   **Feb 2020-Present**

Working on product development for mobility and HVAC applications. Tasks include but are not limited to

- Working with the lead power electronics engineers on design, prototyping and testing of a FOC based BLDC controller.
- Performed comparative analysis of different control schemes to obtain the optimal scheme specific to the application based on the drive cycle of the motor in PLECS.
- Extensively designed PCBs for controllers and auxiliary circuits, component selection, release to fabrication and controller testing.
- Created an RMxprt simulation to obtain the performance profile that can be used to validate the obtained performance.
- Working to improve the design of new versions of the motors which involves assembly and testing of the motors and failure analysis.

Graduate Student Researcher in Power Electronics Lab, UTD   **Nov 2018 - Present**

- Working on the design of a 7kV, 25kW resonant DC-DC converter using SiC devices for MVDC integration of large PV parks. Multi objective optimization is performed to obtain the optimal design for the Medium Frequency transformer and the resonant tank. Currently working on the prototype development.
- Designed a DC-DC converter for a 30kW SiC based Extreme Fast Charger for Electric Vehicles. The configuration of the DC-DC stage is designed to have a reconfigurable output rectifier stages which can be used to charge commercial EVs with both 400V and 800V battery packs.

- Worked on Conducted EMI reduction of IP0P (Input Parallel & Output Parallel) Dual Active Bridge (DAB) DC-DC converter system. Conducted EMI analysis for different Modulation strategies used in the IPOP DAB converter. Common-mode current reduction through noise source and noise path duplication. Hardware validation through 10kW 2 kV-400 V DAB prototype, designed for aerospace application.
- Working on fabrication and testing of a 30kVA Grid connected SiC based inverter.

Graduate Thesis

The objective of the thesis is to investigate the MVDC collection for large Photovoltaic (PV) parks using a DC-DC converter. Proposed an LLC resonant based isolated DC-DC converter for MVDC integration of large PV parks. Used a Multi-objective design optimization-based approach to obtain an optimal design of the resonant tank and Medium Frequency Transformer (MFT). The obtained design was fabricated and a peak efficiency of 99.5% was achieved using the prototype. Working on the design of a feedback-less digital control scheme to enable the synchronous rectification of the medium voltage side devices. Converter is realized using SiC devices. The optimization algorithm and the control scheme are being designed to be used for other applications like MEA, EVs, Battery charging etc., with minimal to no changes.

Academic projects: Sensorless control of PM Motor, Reduction of common mode voltage in a 3 level NPC, Sensorless control of an IPM, Design of Delta & Vienna rectifiers, Comparison of NPC, ANPC & FC type inverters.